I&EC research
Industrial & Engineering Chemistry Research
pubs.acs.org/IECR
Article

Dynamic Modeling of the Reactive Side in Large-Scale Fluidized Bed Boilers

Guillermo Martinez Castilla,* Rubén M. Montañés, David Pallarès, and Filip Johnsson

Cite This: *Ind. Eng. Chem. Res.* 2021, 60, 3936−3956
Read Online
ACCESS | Metrics & More | Article Recommendations

ABSTRACT: This work presents a dynamic model of the reactive side of large-scale fluidized bed (FB) boilers that describes the in-furnace transient operation of both bubbling and circulating FB boilers (BFB and CFB, respectively). The model solves the dynamic mass and energy balances accounting for the bulk solids, several gas species, and the fuel phase. The model uses semi-empirical expressions to describe the fluid dynamics, fuel conversion, and heat transfer to the furnace walls, as derived from units other than the studied ones. The model is validated against operational data from two different industrial units: an 80 MW CFB and a 130 MW BFB, both at steady-state and transient conditions. The validated model is used to analyze: (i) the performance of the reactive side of two FB boilers under off-design, steady-state conditions of operation; and (ii) the open-loop transient response when varying load or fuel moisture. The results underline the key role of heat capacity on the stabilization time. Within a given unit, the differences in heat capacity between the top and bottom of the furnace affect also the stabilization times, with the furnace top (lower heat capacity) being 1−3 times faster in the CFB unit and up to 10 times faster in the BFB unit. Due to the differences in gas velocity, the investigated boilers are found to stabilize more rapidly to input changes when running at full load than at partial load. Lastly, a variable ramping rate analysis shows that the inherent transient responses of the reactive side disappear when disturbances are introduced at (slower) rates, typical of industrial operation. Thus, the reactive side could be modeled as pseudo-static.

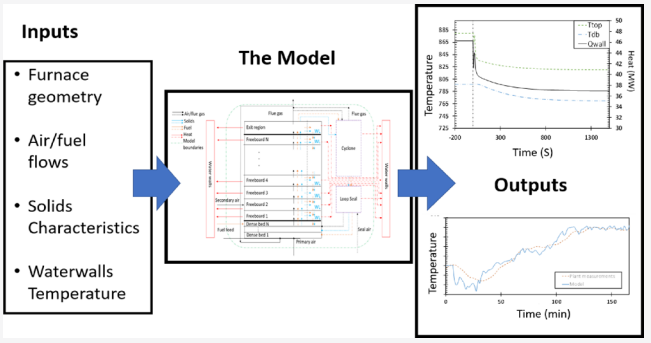

1. INTRODUCTION

Fluidized bed combustion (FBC) units are characterized by strong mixing and heat transfer capabilities, which make them the preferred option for the thermochemical conversion of low-grade and/or renewable solid fuels, such as municipal solid waste and biomass. This means that FBC units have a high level of fuel flexibility, allowing co-firing of different fuel mixtures depending on fuel price and availability. Moreover, fluidized bed (FB) boilers offer higher combustion and generation efficiencies, as well as lower SO_2 and NO_x emissions (achieved through in-bed capture and primary measures, respectively), as compared to other industrial-scale alternatives. Consequently, FB boilers have gained global recognition in the past decades as a viable technology for the thermal conversion of solid fuels and play crucial roles in many energy systems across the world.[1,2] In particular when operated with biomass and renewable waste fractions, FB boilers represent a viable alternative to conventional coal boilers. In markets where combined heat and power (CHP) plants are well-established, replacing old grate or pulverized coal-fired boilers with FB boilers creates the possibility to implement polygeneration facilities that are capable of providing flexible shares of sustainable heat, power, and transportation fuels. FBC units can be categorized as circulating or bubbling (CFB or BFB, respectively), depending on the level of solid entrainment. CFB systems operate at higher excess gas velocities (and typically apply finer solids) than BFBs, resulting in a large fraction of solids being entrained by the gas up through the furnace, with the consequence that a large proportion of these solids exit the furnace. These solids are separated in a primary cyclone and fed back to the furnace through the cyclone dipleg, sometimes passing an external particle cooler. Thus, the CFB is more flexible than the BFB in terms of heat transfer allocation, allowing a wider range of fuels to be burnt in the same unit. There is also a significant level of recirculation of solids within the furnace in the form of a down-flow of back-mixed solids at the furnace walls, making particle convection an important mechanism for heat transfer

Received: December 23, 2020
Revised: February 17, 2021
Accepted: February 17, 2021
Published: March 3, 2021

https://dx.doi.org/10.1021/acs.iecr.0c06278
Ind. Eng. Chem. Res. 2021, 60, 3936−3956

to the water side. In contrast, BFB units are operated at lower excess velocities, such that the quantity of solids carried by the gas flow is not significant, leading to furnaces with very low concentrations of solids above the splash zone, where radiation governs the heat transfer. At present, the capacities of industrial FBC installations range from 10 MW_{el} to around 500 MW_{el} in single units, with CFB boilers having the largest capacities (due to their superior heat transfer flexibility) and being primarily used for power generation; BFB units are typically smaller and are applied in CHP schemes in district heating systems including waste incinerators (around 100 MW).[1]

Biomass and renewable waste fractions used as fuels are characterized by large variations in composition, both between the different fuel types and within a given type of fuel, e.g., in terms of moisture content and, thereby, the heating value. Depending on the extents of these variations, it is more or less challenging to control the temperature field and heat transfer within a given furnace. Furthermore, FBC units are often commissioned in energy systems with a large penetration of non-dispatchable electricity in the form of wind and solar power (making up an increasing share of energy markets worldwide[3,4]). In such cases, the flexibility of operation is attributed a higher value with the aim of following the variability in the net load (demand minus generation by the non-dispatchable electricity generation)[5] since operating costs of wind and solar generation are typically the lowest and will therefore be regarded favorably on the electricity market. However, during time periods with low levels of wind and solar generation, electricity prices increase and thus potentially make thermal electricity generation (or CHP), which can handle load changes and stop and start-ups, profitable. Lastly, some of these boilers provide heat in the form of steam to nearby industrial facilities. This adds a new source of variations that originate from the industrial process itself. Therefore, understanding and analyzing the transient operation of thermal power plants have become important topics in recent years.

Dynamic modeling is an essential tool for the design of energy conversion systems, as it can be used to predict the transient behaviors of boilers and process configurations (including operational and control strategies) under varying conditions.[6] Dynamic models can be used to assess the flexibility of a specific furnace or power plant in order to, for instance, provide insights for dispatch planning. In addition, dynamic simulations can be used in existing plants for the training of plant operators and for process optimization. The terminology "digital twin" has recently arisen when dynamic models can lead to the development of high-fidelity representations of a certain plant. Lastly, dynamic models of combustion units can be integrated into dynamic process models of the entire plant, allowing for investigations of the interactions between the in-furnace side and the water side.

Several comprehensive models have been formulated in the literature to describe and study the FB combustion process, with most of these models focusing on describing steady-state operation. The presence of solids within the boiler has crucial impacts on most of the key parameters and mechanisms, such as temperature and heat transfer. With respect to the fluid dynamics of the gas−solids, Gómez-Barea and Leckner[7] classified the models for FB reactors according to the following approaches: (i) computational fluid-dynamics (CFD) models, which solve the transport equations for mass, momentum, and energy for both phases; (ii) fluidization models (FMs; also known as semi-empirical models), which do not solve the momentum equations but use simplified means (semi-empirical correlations, assumptions, simpler models) to obtain the velocity fields and, thereafter, solve the mass and heat balances; and (iii) black-box models (BBMs), which do not offer spatial resolution and apply empirical correlations that respect the overall mass balances over the reactor (assuming, in some cases, chemical equilibrium). Furthermore, FMs can be divided into three groups according to the type of spatial discretization used: (i) one-dimensional (1D), which discretizes the unit in the vertical direction;[8−10] ii) quasi-2D models (often called 1.5D), which develop the 1D approach for CFB units by splitting each cell into core and annulus regions;[11,12] and (iii) detailed 3D models.[13]

Regarding the dynamic models of FB combustors, most of those available in the literature focus on the water side, such that the description of the reactive side is outside the scope. The heat transferred from the gas side has frequently been modeled as a first-order function of the power demand. This reflects the relative scarcity of knowledge regarding the gas−solid dynamics inherent to the FB furnace, which can be attributed to the complexity of the field and the lack of measurements made under conditions relevant to industrial units. As for the dynamic models of the reactive side in FBC units reported in the literature, the focus has been on CFB units. Park and Basu[14] presented a simplified FM with a 1D description of the furnace that is capable of predicting the transient concentrations of oxygen and char measured in a 0.3 MW unit when the fuel feed rate is changed. Majanne and Köykkä[15] split the furnace model into nine control volumes that are connected to a model of the water-steam cycle. The model has been used to simulate the variations in steam production that occur after a change in the fuel moisture level, revealing a local dip in the steam mass flow before reaching a stable state after 10 min. Chen and Xiaolong[16] described a 1.5D FM of a CFB unit, which, after steady-state validation against a 410 t/h pyroflow coal unit, was used to simulate changes in the fuel feed and track the dynamic responses of the systems. As in the study carried out by Park and Basu,[14] the aim was to analyze these responses qualitatively. These two studies have congruent conclusions: the oxygen concentration and the steam drum pressure decrease following an increase in the coal feed rate while keeping constant the combustion air flow. Kim et al.[17] used an FM (validated against steady-state experimental data from a 795 MW_{th} unit[18]) to understand the implications that different operational changes have for the dynamics of the main process variables of CFB boilers (e.g., the solids circulation rate). The study of Kim et al.[17] focused on the effects of the solid flow on the transient responses of the CFB loop, revealing overshoots in the temperature responses, as well as strong effects of solid size and inventory on the temperature responses. Most recently, Peters et al.[19] published a core-annulus dynamic model. The model was used to resemble fast load change measurements from a 1 MW pilot unit. Some other groups have focused on the development of dynamic models of CFB boilers with the aim of designing effective control structures. Findejs et al.[20] presented a 1D model using empirical correlations derived from experiments conducted in a pilot unit, with the goals of developing a model-based control strategy and helping the controller to predict the boiler responses of power output, oxygen concentration, and bed temperature over several minutes. Findejs et al.[20] concluded that PID controllers are not adequate and, given

https://dx.doi.org/10.1021/acs.iecr.0c06278
Ind. Eng. Chem. Res. 2021, 60, 3936−3956

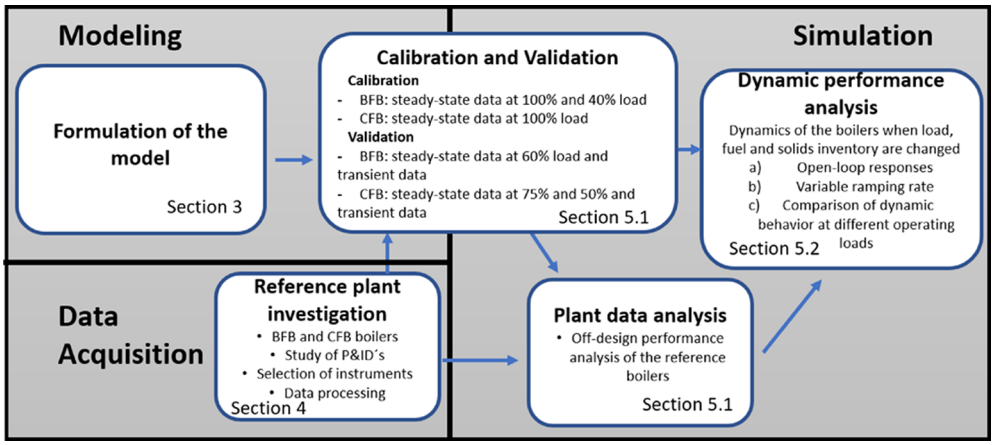

Figure 1. Overview of the applied methodology. Data acquired from industrial units are used to calibrate and validate the model. The validated model is used to perform investigations of partial load operation and the dynamic response to changing the inputs.

the high level of interaction between the variables, suggested the use of a multiple-input-multiple-output (MIMO) technology. Zimmerman et al.[21] developed a black-box dynamic model of a waste CFB boiler that included the water side and validated it against the dynamic data obtained from a 160 MW unit. When the model was applied to test different control strategies, it showed that model predictive control with feedforward gave the best results. Regarding BFB units, the literature on dynamic models is scarce. Kataja and Mojanne[22] presented a model of a BFB boiler that splits the furnace into four control volumes and includes the water side. Experimental validation of the model was made with the drum and steam pressure, and the model was used to simulate a step-change in fuel flow and to track the variations in gas temperature and steam flow. Selcuk and Degirmenci[23] carried out a modeling study of the dynamics in BFB boilers, together with validation against transient and steady-state data on the O_2 and CO concentrations, as well as the gas temperatures measured in a 0.3 MW unit. The results of the simulation showed that the transient responses of CO were smoother than those of O_2, as well as that when the air flow rate was increased the char inventory in the dense bed was decreased temporarily, due to elutriation. Surasani et al.[24] developed a model for biomass combustion in bubbling units that were validated against steady-state measurements from a laboratory scale reactor, concluding that the model was suitable to be integrated into further plantwide models. Most recently, Suárez-Almeida et al.[25] presented a dynamic model of an FB gasifier validated against transient experiments at a laboratory scale and applied it to investigate the dynamic behavior of the system under a start-up and a load change.

Considering the abovementioned studies, the following can be concluded regarding the dynamic modeling of FB boilers:

(i) Most of the models abovementioned are unit-specific, i.e., they have been calibrated to predict the dynamic behavior of a specific reference combustor. Therefore, models are lacking that are built in a generic way so that they are capable of simulating different boiler sizes and designs, operational ranges, and fuel types.

(ii) Most of the available models have been validated with pilot-scale units rather than with large-scale plants.

(iii) The few studies that have included experimental validation at industrial size ([16,17,21]) have performed the validation exclusively at nominal load under steady-state conditions.

Therefore, there is a lack of general knowledge about the dynamic behavior of the reactive side of large-scale boilers.

The aim of the present work is to provide insights into the dynamics of the reactive in-furnace (flue-gas) side of large-scale FB boilers. For this purpose, a dynamic model of large-scale FB combustors that takes into account the heat transfer, combustion, and a 1.5D description of the fluid dynamics is developed, which is capable of simulating both BFB and CFB conditions. The model is validated and used thereafter to study different scenarios defined by changes in the input data. To enable the model to provide satisfactory descriptions within wide ranges of operation (load, fuel type, fluidization velocity, bed material properties, etc.) and for different boiler sizes and geometries, the semi-empirical expressions used are derived with the ambition to be as generic as possible: based on the underlying physical mechanisms, fit to experimental data covering wide spectrum of input variables, and taken in units other than the two used for the validation in this work (as opposed to simply correlating experimental data from specific runs and/or units). The model is validated against the operational data for the reactive side obtained from two industrial units, a BFB and a CFB, whereby the validation data were sampled at different load levels for both steady-state and transient operation. Once validated, the model is used to simulate and compare the dynamic responses of the two boilers under varying boundary conditions (load, fuel composition, solids inventory). The present dynamic reactor model is formulated with the ambition to integrate it into dynamic process models of the water side in the future.

2. METHODOLOGY

Figure 1 presents a schematic of the methodology followed in the present work, divided into three main parts: modeling, data acquisition, and simulation. The modeling part contains the mathematical description of the in-furnace dynamics (Section 3). The data acquisition part contains in-depth descriptions of the reference plants and instruments used for sampling the data and for the data processing (Section 4). The acquired data are used to calibrate and validate the model (Section 5.1), which are tasks that fall within both the model build-up and simulations, as model runs are used to improve the model formulation. Measurements made under steady-state con-

https://dx.doi.org/10.1021/acs.iecr.0c06278
Ind. Eng. Chem. Res. 2021, 60, 3936−3956

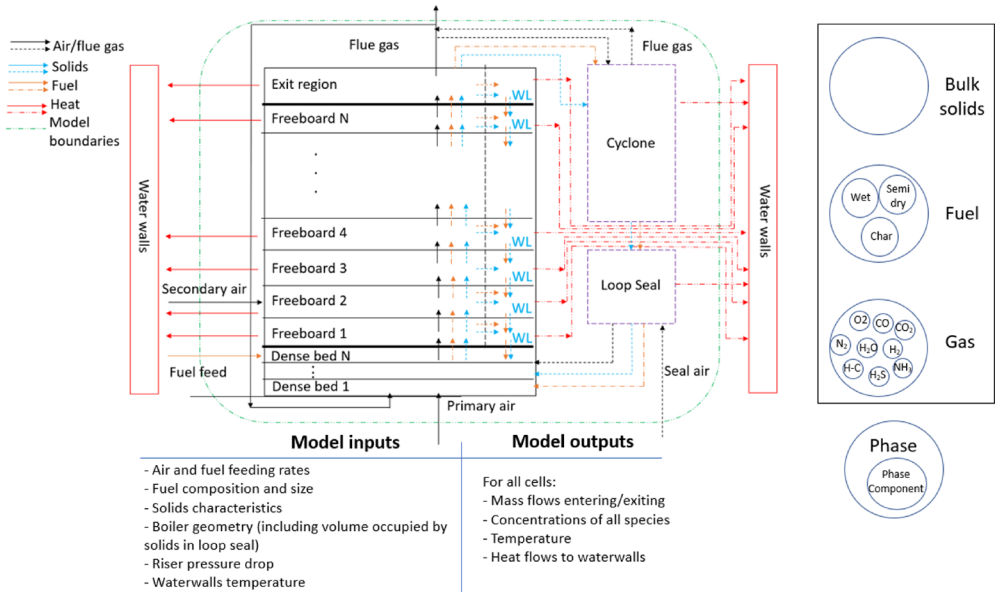

Figure 2. Schematic of the model including the domain discretization, scheme of the phases and phase components that are accounted for, and the lists of model inputs/outputs. Convective mass flows are shown together with the heat transferred to the non-insulated domain boundaries. The dotted lines/arrows apply exclusively to CFB conditions.

ditions are used for model calibration, while the data sampled under transient conditions (and even under steady-state partial load) are used for validation of the dynamic model. The modeled data resulting from the calibration and validation are used to study the off-design (partial load) performance of FB boilers (see Section 5.1). Finally, dedicated simulations are carried out to study the dynamic open-loop response (i.e., the uncontrolled response of the system when a specific input is suddenly changed) after changes to the fuel composition and load, including a variable ramping rate analysis (see Section 5.2). This study utilizes results from the off-design performance analysis to aim the understanding of the inherent dynamics of the units.

Deviations between the model output and the operational data are quantified as absolute percentage errors, AP (see eq 1), between the modeled, x_m, and measured value, x_p.[26] After a change is introduced, the dynamic analysis of a process variable, y_0, to its new steady-state value, y_∞, is defined by the relative change, RC (see eq 2), and stabilization time, t_s (computed as the time required to complete 90% of the change; see eq 3).

$$\mathrm{AP} = 100 \times \left| \frac{x_m - x_p}{x_p} \right| \tag{1}$$

$$\mathrm{RC} = 100 \times \frac{y_\infty - y_0}{y_0} \tag{2}$$

$$t_s = \tau \rfloor_{y_0 \to y_\infty \mp 0.1(y_0 - y_\infty)} \tag{3}$$

3. DESCRIPTION OF THE MODEL

The model presented in this paper describes the reactive side of FB boilers (including combustion, heat transfer and fluid dynamics) through a number of perfectly mixed control volumes exchanging mass and energy and for which the coupled dynamic balances of those scalars are solved. This generates a set of differential and algebraic equations. The model has been implemented in the open modeling language Modelica.[27]

3.1. Model Structure.

A schematic representation of the model is given in Figure 2. The domain is divided into the following regions identified from previous experimental studies:[28−30] dense bed, freeboard, exit zone, cyclone, and loop seal. Those regions known to exhibit significant gradients of concentration or temperature, i.e., to deviate from the perfectly mixed assumption made for the constituent control volumes (e.g., the dense bed or the freeboard) are consequently described as a sequence of a number of stirred-tank reactors. In this work, a balance between spatial resolution and computational cost was pursued, and consequently, the number of cells was increased until the addition of a cell did not change the exit gas concentration more than 0.5%, resulting in a discretization of the dense bed and the freeboard into 3 and 12 vertical cells, respectively, for the reference cases here modeled.

The model accounts for three mass phases: bulk solids, fuel, and gas (see Section 3.2). The convective mass flows between the cells are shown in Figure 2 (dotted lines indicate mass flows that are significant only under circulating conditions; see Section 3.4). Also shown in Figure 2 are the heat exchanges between the gas−solid suspension and non-insulated domain boundaries (waterwalls), which are also included in the model.

The inputs to the model are (i) the boiler geometry (including inputs required for fluid dynamic computations, see Section 3.3.1); (ii) the mass flows, compositions, temperatures and locations of the injected streams (gas—air in this work—and fuel); and (iii) the bulk solids properties (size and density). In case the modeled furnace has tapered walls, the cross-sectional area of each cell can be defined individually so that the impact of the inclined walls on the solid inventory in each cell as well as on the gas velocity can be accounted for. Since the scope of this work is limited to the reactive side, the temperature of the furnace walls is considered a thermal boundary condition and, thus, is a known model input. The waterwall temperature is assumed to be constant and equal to

https://dx.doi.org/10.1021/acs.iecr.0c06278
Ind. Eng. Chem. Res. 2021, 60, 3936−3956

the water-side temperature, based on several studies of boilers operated at variable load under live steam pressure control mode (see, for example, ref 31). For refractory-lined regions, a wall boundary condition of zero heat flux is set, i.e., the wall temperature is set as equal to that of the corresponding control volume of the in-furnace side. As outputs, the model provides for all the control volumes, concentrations, compositions, and mass flows of the different phases considered (solids, fuel, and gas), and the temperature and heat flow transferred to the neighboring cells or walls.

3.2. Definition of the Phases and Phase Components. The model considers three phases: gas, bulk solids, and fuel. The gas phase is modeled as an ideal gas mixture that consists of nine phase components (or species): nitrogen (N_2), oxygen (O_2), carbon monoxide (CO), carbon dioxide (CO_2), water vapor (H_2O), hydrogen (H_2), ammonia (NH_3), hydrogen sulfide (H_2S), and hydrocarbons ($C_aH_bO_c$). The specific enthalpy values for all these species are computed through polynomial expressions.[32]

For the bulk solids, in order to reduce the complexity, the model disregards the modeling of poly-dispersed solids and corresponding attrition and size segregation phenomena and assumes mono-dispersed spherical particles with a particle size that is provided as an input. The solids density ρ_s is also given as an input (2600 kg/m^3 for silica sand, which is the bed material used in this work). The solids enthalpy is calculated from the specific heat capacity, $c_{p,s}$ (the heat of formation does not play any role since it is assumed that the bulk solids do not participate in any reactions).

Regarding the fuel phase, to account for the changes in size and density that occur during conversion, several phase components (or fuel classes) are characterized according to size, density, and conversion mechanism. For fuel particle sizes typical of FB conversion (i.e., greater than mm-scale), drying and devolatilization are partially overlapping, with a certain delay in the start of the latter and simultaneous completion.[33] According to this scheme, the first fuel class accounts for the fresh fuel, while the second one represents the fuel at the start of devolatilization (a fraction of the moisture, typically 10−20%, has already been released with the corresponding decrease in density, while the particle size remains the same). For the volatiles, a typical composition[34] is assumed, and heat and elementary mass balances are applied to calculate the three hydrocarbon indices ($C_aH_bO_c$) fulfilling the ultimate analysis and the heating value of the fuel given as inputs. Finally, the third class represents the fuel after all moisture and volatiles have been released (the density is calculated consequently), i.e., the char particles. An accurate description would demand representation of the char through several conversion classes (see ref 35). However, this would in turn require a description of the fuel fragmentation, which is a complex phenomenon that is highly fuel-dependent and typically not straightforward to characterize. Thus, a pragmatic approach is taken here in defining a single conversion class for the char and setting its average size at 3 mm.[36]

3.3. Mass and Energy Balances. The generic dynamic mass balances in a cell i for the components in each of the three phases defined—bulk solids, fuel, and gas—are expressed by eqs 4, 5, and 6, respectively. The source term s represents the net generation of the given phase or phase component and is absent for bulk solids, as these are assumed to be inert in this work. The summing is done over all the incoming/outgoing flows.

$$\frac{\mathrm{dm_{s,i}}}{\mathrm{d}t} = \sum \dot{m}_{\mathrm{in},s,i} - \sum \dot{m}_{\mathrm{out},s,i} \tag{4}$$

$$\frac{\mathrm{d}m_{f,k,i}}{\mathrm{d}t} = \sum \dot{m}_{\mathrm{in},f,k,i} - \sum \dot{m}_{\mathrm{out},f,k,i} + \sum s_{f,k,i} \tag{5}$$

$$\frac{\mathrm{d}(m_{g,r}X_{k,r})}{\mathrm{d}t} = \sum \dot{m}_{\mathrm{in},g,i}X_{\mathrm{in},k,i} - \sum \dot{m}_{\mathrm{out},g,i}X_{k,i} + \sum s_{g,k,i} \tag{6}$$

The energy balance in a cell i is shown in eq 7, where k refers to all the phase components considered, j represents the heats of reaction/phase change, $Q_{\mathrm{extracted}}$ stands for the heat extracted by the waterwalls, and Q_{rad} includes the net emitted/absorbed radiative heat, if such exists.

$$\begin{aligned}\frac{\mathrm{d}E_i}{\mathrm{d}t} &= \frac{\mathrm{d}(m_i c_{p,i}(T_i - T_0))}{\mathrm{d}t} \\ &= \sum \dot{m}_{\mathrm{in},k,i}q_{\mathrm{in},k,i} - \sum \dot{m}_{\mathrm{out},k,i}q_{\mathrm{out},k,i} + \sum s_{j,i}Q_{j,i} \\ &\quad - Q_{\mathrm{extracted},i} + Q_{\mathrm{rad},i}\end{aligned} \tag{7}$$

The different terms constituting the mass and energy balances formulated above are governed by three processes: fluid-dynamics, thermochemical conversion, and heat transfer. These aspects are covered in the following subsections.

3.3.1. Fluid Dynamics. Regarding the gas flow, a plug-flow approach is used to capture the vertical gradient of gas composition across the furnace, i.e., no dispersive transfer is allowed between the control volumes. It is also assumed that, based on previous findings,[37] there is no gas flow in the wall layers of a CFB freeboard, and in regions with secondary air injection, the air is assumed to join the upward flow in the core.

The solid concentration in the dense bed is by definition constant, and is here calculated according to expressions provided in the literature.[11] The total riser pressure drop (handled as an input, see Figure 2) is assumed constant during operation. As a consequence of this, the dense bed height, H_0, is constant, which allows to keep the grid size invariant over time. For an evaluation of the effect of changes in solid inventory on the furnace dynamics, see Section 5.2. The axial mixing of solids,[38] including the fuel,[39] in the dense bed is known to be very high, which is implemented in the model through a sufficiently enough dispersion coefficient that ensures perfect vertical mixing.

The solid flow in the freeboard is studied in the literature by typically focusing on the bulk solids, such that relatively little is known about the fuel flow.[11] The present model assumes that the expressions derived for the bulk solids (typically using the terminal velocity as the characteristic variable) also apply to the fuel particles. The solid flow in the CFB freeboard has been modeled in accordance with Johnsson et al.,[40] i.e., the vertical profile of the solids concentration consists of two exponential decays (see eq 8) linked to two back-mixing mechanisms. First, a splash zone with strong solid back-mixing (characterized by a decay coefficient a in eq 9[30]) dominates the lower freeboard immediately above the dense bed. In parallel with this, the gas may entrain solids (a significant share under CFB conditions) to locations higher in the riser. The amount of solids entrained from the bottom region into the transport zone is characterized as a concentration, $c_{s,\mathrm{entr}}$, which is calculated using an empirical correlation derived from the data presented by Djerf et al.[41]

https://dx.doi.org/10.1021/acs.iecr.0c06278
Ind. Eng. Chem. Res. 2021, 60, 3936−3956

(see eq 10). This data is, to the knowledge of the authors, the one best depicting the solids entrainment phenomena in industrial-sized units. The entrained solids are assumed to flow at their slip velocity, $u_s = u - u_t$, with u_t being the single particle terminal velocity (calculated according to[42]), and form a transport zone that extends up to the riser top and that shows a constant net back-mixing from the core to the wall layers. This back-mixing is governed by a mass transfer coefficient, k, computed from measurements in large-scale units under a wide range of operational conditions and boiler geometries,[9,30,40,41,43−46] as shown in eq 11. This back-mixing yields an exponential decay with a decay constant K (linked to k according to eq 12, see ref 34). To describe this, the model discretizes the CFB freeboard following a 1.5D approach, i.e., a core/annulus structure is considered in which both the gas and solids flow upwards in the core cells, whereas the solids flow downward in the annulus cells (forming wall layers along the furnace walls) (Figure 3). According to this, the net flow of

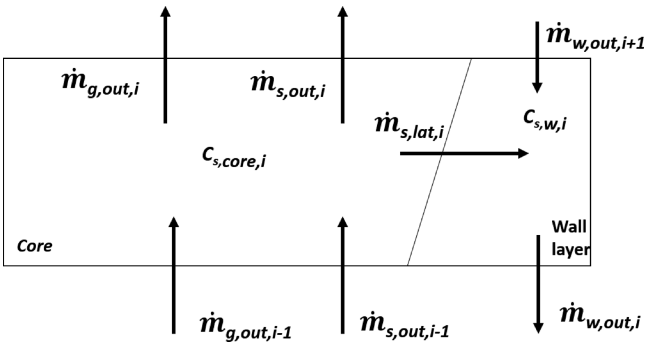

Figure 3. Schematic representation of the mass flows and concentrations of a vertical element of the core/annulus structure. The solid phase flows in the downward direction in the wall-layer cells, whereas the solids and gas phases flow in the upward direction in the core.

solids from a certain cell i with height dz to the neighboring wall layers is given by eq 13, yielding an exponential decay of the solid concentration with height, see K (eq 12).[40] Note that eq 8 is derived from the integration of the solid concentrations across the vertical elements of the furnace, as the one depicted in Figure 3.

$$c_s(h) = (c_{s,0} - c_{s,\mathrm{entr}}) \times \exp(-a(h - H_0)) + c_{s,\mathrm{entr}} \times \exp(-K(h - H_0))\ h > H_0 \tag{8}$$

$$a = 4\frac{u_t}{u} \tag{9}$$

$$\frac{c_{s,\mathrm{entr}} \times (u - u_t)}{\rho_g u} = 3109 \times \left(1 - \frac{u_t}{u}\right)^{6.8} \tag{10}$$

$$k = 0.1084 \times (u - u_t) \tag{11}$$

$$K = \frac{4k}{D_e(u - u_t)} \tag{12}$$

$$\dot{m}_{\mathrm{lat},i} = A_i c_{s,\mathrm{entr}}(u - u_t) \times \exp(-K(h - H_0))Kdz \tag{13}$$

Regarding the concentration of solids within the wall-layer cells (important for the heat transfer to the waterwalls as described in Section 3.3.3), eq 14 is used. The solids in the wall layers are assumed to flow at the solid terminal velocity, in line with the results obtained from velocity measurements in large-scale boilers.[47] The wall-layer thicknesses (and, thereby, the volumes of the corresponding cells) decrease with height and are calculated by means of an empirical correlation (eq 15) derived from experimental data from several large-scale boilers.[48] The thickness is then used to calculate the cross-sectional area A_w.

$$\dot{m}_{w,\mathrm{out}} = A_w \times c_{s,w} \times u_t \tag{14}$$

$$\frac{t_{\mathrm{wall}}}{D_{eq}} = 0.55\mathrm{Re}_t^{-0.22}\left(\frac{H_0}{D_{eq}}\right)^{0.21}\left(\frac{H_0 - h}{D_{eq}}\right)^{0.73} \tag{15}$$

At the top of the riser, the solids experience a so-called backflow effect, resulting in that only a share of the upward-flowing solids exit the furnace to the cyclone. The remaining solids are back-mixed to the wall layers.[28,29] This share can be expressed by the backflow coefficient k_b, computed in the model as a function of the Stokes number according to eq 16 obtained from measured data published in ref 41. Similarly, as for the equation describing the solids entrainment, this expression has been obtained from data measured in a single unit and is here extrapolated to describe other boilers.

$$k_b = 0.85\left[\frac{1}{1 + \exp(-66St)}\right]^{255} \tag{16}$$

The solid residence time in the cyclone is calculated according to ref 49. The bed voidage in the loop seal (typically in the range of 0.5−0.6) is modeled according to expressions for bubbling beds,[11] which combined with the solid circulation flow gives the average residence time for the solids.

Finally, for the sakes of simplicity and decreased computational costs, the volume occupied by the fuel phase is neglected in the mass balances, i.e., only the gas and the bulk solid phases are taken into account, i.e., $\varepsilon_s + \varepsilon_g = 1$. This should be a reasonable assumption given that the average volume fraction of a fuel is typically in the order of 10^{-3}, with maximum local values (in the bottom region of BFB units) in the order of $1-5 \times 10^{-2}$.

3.3.2. Thermochemical Conversion. The generation and consumption rates of the fuel class (phase components of the fuel phase) n are computed according to eqs 17 and 18, with $X_{n-1,\mathrm{rel}}$ being the mass fraction of the foregoing class converted to the gas phase (for details, see ref 35). Each class has a characteristic time related to its thermochemical process, i.e., drying, devolatilization, and char combustion. Note that the difference between the consumption and generation rates of a certain fuel class constitutes the source term used in the mass balance given in eq 7.

$$s_{n,\mathrm{consum}} = \frac{m_n}{t_{n\to n+1}} \tag{17}$$

$$s_{n,\mathrm{gen}} = s_{n-1,\mathrm{consum}} \times (1 - X_{n-1,\mathrm{rel}}) \tag{18}$$

The initial conversion steps, drying and devolatilization, are purely thermal. Thus, for standard FB conditions operating with large solid fuel particles, it is usual to estimate the

https://dx.doi.org/10.1021/acs.iecr.0c06278
Ind. Eng. Chem. Res. 2021, 60, 3936−3956

Table 1. Rate Expressions for the Homogeneous Reactions Considered in the Model

reaction	rate of conversion
$CO + \frac{1}{2}O_2 \rightarrow CO_2$	$K_{eff,CO} \times C_{CO} \times C_{O2}^{0.5} \times C_{H2O}^{0.5}$ (21)
$H_2 + \frac{1}{2}O_2 \rightarrow H_2O$	$K_{eff,H2} \times C_{H2}^{3/2} \times C_{O2}$ (22)
$C_aH_bO_c + \left(2a + \frac{b}{2}\right)O_2 \rightarrow aCO_2 + \left(\frac{b}{2} + c\right)H_2O$	$K_{eff,C_aH_bO_c} \times C_{C_aH_bO_c}^{0.5} \times C_{O2}$ (23)

combined drying and devolatilization time as a function of the particle diameter, as expressed in eq 19.[50]

$$t_{dry+dev} = 1.3 d_p^{1.6} \tag{19}$$

Based on the findings published in ref 51, it is assumed that 10% of the combined drying and devolatilization time is allocated as only-drying time (conversion time of the first fuel class), whereas 90% is simultaneous drying and devolatilization time (conversion time of the second fuel class). For a certain cell i, the characteristic time for the third class, char, is calculated according to the shrinking sphere model under transport-controlled conditions, typical for an FB fuel, as shown in eq 20. Note that this value is computed at each time step in each cell.

$$t_{char,i} = \frac{\rho_{char} d_{p,char}^2}{8\Omega M_{char} D_{A,B} C_{O2,i}} \tag{20}$$

The homogeneous reactions accounted for in the model are listed in Table 1, together with the expressions for their effective rates (eqs 21−23). In the latter, the reaction coefficient K_{eff} includes both the effect of kinetics (through the concentration dependencies from refs 52 and 53) and the effect of gas mixing (through the calibration of the values of K_{eff}, see Section 5.1), with the latter being the driving mechanism in FB combustors. The heats of reaction are taken from a previous paper.[54]

3.3.3. Heat Transfer to the Walls. Bed-to-wall heat transfer in FB units occurs through convection and radiation (with the contribution from convection increasing with increases in the solids concentration). While most of the studies in the literature report effective heat transfer coefficients that lump together both convection and radiation, an accurate description should treat them separately.[55] In this work, heat transfer to surfaces other than the waterwalls, i.e., internal tubes or tube bundles, is not modeled but is taken into consideration in the corresponding control volume as a heat sink, the magnitude of which is taken as an input.

The convective heat transfer coefficient is modeled according to eq 24.[55] The presence of solids in the freeboard (even at volumetric concentrations as low as 10^{-3}) represents an optical thickness and implies that there is a significant contribution of the solids to radiative heat transfer. To account for this, the model introduces the radiation efficiency factor η_{rad}, as suggested previously,[55] according to which the radiation of heat from the core solids to the waterwalls increases with a decrease in solid concentration. When operated under circulating conditions, the total heat transfer to the wall in a specific cell i is formulated as in eq 25.

$$h_c = 25 c_s^{0.58} \tag{24}$$

$$Q_{extracted,i} = h_c A_w (T_{wl} - T_w) + \eta_{rad} \varepsilon_{susp,i} A_w \sigma (T_c^4 - T_w^4) \tag{25}$$

At gas velocities typical for BFB operation, the velocity is not sufficiently high to drag solids into the freeboard for the solids to make a significant contribution to the convective heat transfer to the walls, which instead is dominated by radiation. The optical thickness generated by this very low concentration of solids in the freeboard may be relevant, but it does not hinder different surfaces (dense bed surface, furnace roof, and walls) from exchanging radiative heat.

In general, net radiative heat over a certain surface element is expressed as the difference between the absorbed and emitted heat:

$$q_{net,surf} = \alpha_w q_{in,surf} - q_{emitted,surf} \tag{26}$$

For a certain surface, surf, the incoming heat $q_{in,surf}$ and heat emitted $q_{emitted,surf}$ are given by eqs 27 and 28, respectively. The first right-hand-side term in eq 27 describes the incoming radiation from other surfaces through their radiosity, geometrical view factor (computed according to[56]), and transmissivity $(1 - \alpha_g)$ along the gas−solid suspension path. The last term in eq 27 represents the incoming radiation from other cells accounting also for the path transmissivity.

$$q_{in,surf} = \sum_j \left((\sigma \varepsilon_j T_j^4 + q_{in,j}(1 - \varepsilon_j)) \times A_j F_{j-surf} \prod_j^s (1 - \alpha_{g,j-surf}) \right) + \sum_k \left(\sigma \varepsilon_{g,k} T_{g,k}^4 A_k F_{k-surf} \prod_k^{surf} (1 - \alpha_{g,k-surf}) \right) \tag{27}$$

$$q_{emitted,surf} = \sigma \varepsilon_w T_s^4 A_{surf} \tag{28}$$

For a volumetric cell, vol, the incoming and emitted radiative flows are expressed according to eqs 29 and 30, respectively. The right-hand-side terms in eq 29 refer to the incoming radiation from other surfaces and cells. Even at low gas velocities characteristic of BFB operation, the freeboard of the furnace contains a small fraction of fine solids. Therefore, the emissivity of the cells is computed using Beer's law, as shown in eq 31, in which k_{vol} is handled in the model as a tuning factor (see Section 5.1).

https://dx.doi.org/10.1021/acs.iecr.0c06278
Ind. Eng. Chem. Res. 2021, 60, 3936−3956

$$q_{\text{in,vol}} = \sum_j \sum_i \left(q_{\text{emitted},j} F_{ji} \prod_k^s ((1 - \alpha_{k,ij}))\alpha_g \right) + \sum_k \sum_i \left(\sigma \varepsilon_{g,k} A_k F_{ki} T_k^4 \prod_h^{\text{surf}} ((1 - \alpha_{h,k\text{surf}}))\alpha_g \right) \quad (29)$$

$$q_{\text{emitted,vol}} = \sigma \varepsilon_{\text{vol}} T_{\text{vol}}^4 A_{\text{vol}} \quad (30)$$

$$\varepsilon_{\text{vol}} = 1 - e^{-k_{\text{vol}} Lp} \quad (31)$$

3.4. Implementation. The present model was developed to simulate FB boilers operating over a wide range of gas velocities. As discussed above, the entrainment of solids into a CFB freeboard results in wall layers (thus requiring a 1.5D discretization of the freeboard), which will govern the heat transfer mechanisms (shifting from exclusive radiation governance to also being governed by a significant contribution from convection). While the formulation of a single general model that is able to describe both designs is feasible, the assumption of a specific (BFB or CFB) mode renders significant simplifications in each formulation, and this translates into substantially decreased computational costs. In addition, CFB units operating at a minimum load, down to 20% in present generation designs, still retain their CFB characteristics (formation of solid wall layers and solid concentrations that are sufficiently high to create an opaque cross section). Thus, the operational window in a given design is not wide enough to cover both BFB and CFB conditions. Table 2 summarizes the above-discussed assumptions for each of the model modes (BFB/CFB).

Table 2. Assumptions and Calibration Factors Applied to the BFB and CFB Model Configurations

	assumptions	calibration factors
CFB mode	presence of solids external circulation loop	gas mixing
	formation of solid wall layers	bulk solid size
	opaque cross section (radiation only between gas−solid suspension and walls)	
BFB mode	negligible solid entrainment from the bottom bed	gas mixing
	negligible convective heat transfer to the walls	absorptivity of the gas−solid suspension

The model proposed here is obviously simplified and semi-empirical in nature while still having the aim to model the complex phenomena that occur in FB boilers. Thus, there is need to calibrate the model with actual measurements. The gas mixing rate governing the homogeneous reactions is typically a calibration factor in FB modeling, including in the present modeling of both BFBs and CFBs. For CFB conditions, the bulk solids size in the unit (which differs from that fed due to attrition and size segregation phenomena in, for example, the cyclone) is also used as a calibration parameter. For BFB conditions, where heat transfer to the walls is assumed to be driven exclusively by radiation, the emissivity of the freeboard cells is highly sensitive to the presence of even minute amounts of solid fines (typically generated by attrition in the dense bed). This concentration of solid fines is complex to model and is here used as a calibration factor through the tuning of the effective absorptivity of the freeboard cells, k_g. Section 5 describes in detail the model calibration.

4. DESCRIPTION OF THE REFERENCE BOILERS

Two industrial boilers, one BFB and one CFB (depicted in Figure 4), were selected as the reference units in this work, i.e., the model is experimentally calibrated and validated against measured data from these boilers and the case studies are based on studying their behaviors. The size, design, and operational conditions of the two boilers are representative of their respective kinds (for a summary of the design data, see Table 3). Both units are operated with wood chips that have the nominal compositions listed in Table 4. Note that two different operational datasets are used for the CFB, each with a different fuel composition.

4.1. Reference CFB Unit. The CFB reference boiler is a CHP plant (80 MW_{th} plus 20 MW_{el}), as depicted in Figure 4a. The boiler, which is one of three units within the district heating system of the city of Karlstad in Sweden,[57] is operated as a mid-merit type of plant. The hot loop consists of a furnace ($8.5 \times 4.1 \times 21.0$ m^3) and two parallel cyclones with corresponding loop seals. The fuel is fed through ports located in the return pipes from the seals back to the riser. The unit has secondary air ports located between 1.5 and 3 m above the bottom gas distributor. The boiler walls are covered by vertical membrane walls, with the lowest region (up to a height of 4.5 m) being refractory lined. One of the superheaters is located inside the furnace in the form of a package of tube bundles at an approximate height (h) of 11 m.

The main control objective variable (CV) in this study is the boiler load, which is part of a larger plant-wide control structure and determines how much heat the boiler produces in the form of steam. This variable is controlled through four manipulated variables (MVs), the feeding rates of the air flows and fuel, which follow a cascade control structure, with the air flow controller being programed to maintain an air-to-fuel ratio of 1.2. The controller output is then corrected with the measured outlet concentration of oxygen. The primary-to-secondary air ratio follows an algorithm previously implemented in the controllers that, in order to avoid defluidization, adjusts the ratio as a function of the boiler load.

4.2. Reference BFB Unit. The reference BFB boiler (Figure 4b) is a 130 MW_{th} CHP unit that acts as a base-load unit in the local district heating network of the City of Örnsköldsvik in Sweden[57] while also supplying steam to a nearby pulp and paper plant. The furnace has dimensions of $9.18 \times 8.67 \times 30$ m^3 and is operated with a dense bed height of around 0.5 m. Secondary and tertiary air flows are fed at heights of 2.5 to 10 m above the grid. Some of the cold flue gas can be recirculated for controlling the bed temperature. The furnace walls and roof are covered by membrane waterwalls, except for the refractory lining of the bottom section (up to a height of 2.5 m). Two superheaters in the form of three tube bundles are immersed in the upper part of the furnace.

The boiler load control follows a strategy similar to that described above for the CFB reference boiler, except that it additionally includes a regulatory bed temperature control, whereby the recirculated flue gas flow (MV) is, if needed, used to reduce the bed temperature (CV).

https://dx.doi.org/10.1021/acs.iecr.0c06278
Ind. Eng. Chem. Res. 2021, 60, 3936−3956

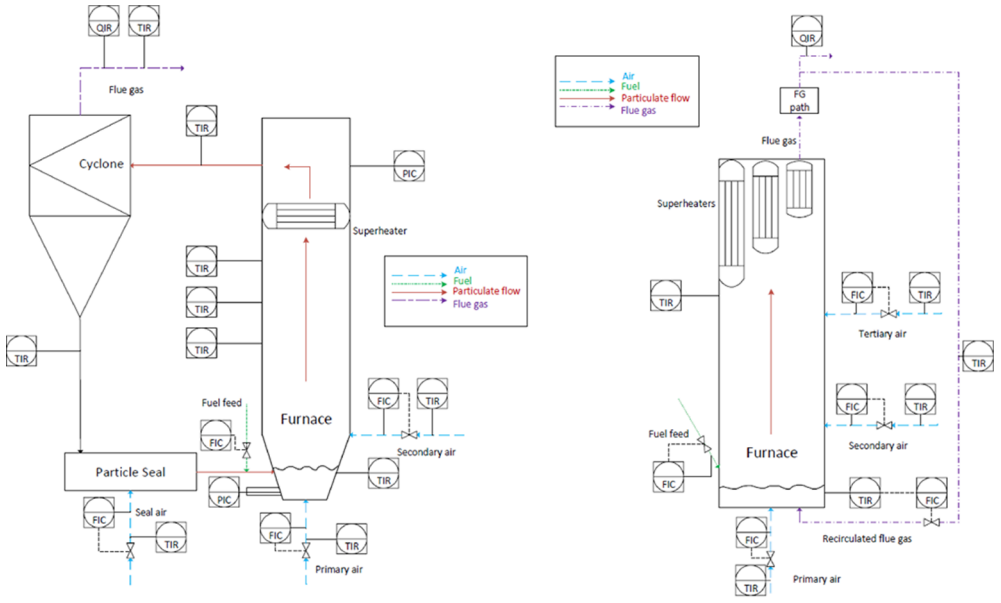

a) CFB unit b) BFB unit

Figure 4. Schematic piping and instrumentation diagram of the (a) CFB reference unit and (b) BFB reference unit. The first letter of each instrument represents the variable measured/controlled: temperature, *T*, flow, *F*, pressure, *P*, and composition, *Q*. The second letter indicates that it is an instrument, and the third letter indicates whether it is a controller (C) or a reading (R).

Table 3. Main Design Parameters and Operating Conditions of the Reference Plants from which the Measured Data Were Obtained

parameter	CFB furnace	BFB furnace
furnace dimensions, m	8.5 × 4.1 × 21	9.18 × 8.67 × 30
waterwalls area, m^2	425	885
cyclone volume, m^3	77.5 × 2	
fuel flow, kg/s	12	13.8
air flow, Nm^3/s	30.6	38
primary/secondary air ratio	0.78	0.74
recirculated flue gas flow, Nm^3/s		14
gas velocity, m/s	4.8	1.2
air inlet temperature, °C	190	260
steam temperature, °C	290	344
heat extracted by furnace superheaters, MW	2.5	18.3
bulk solids density, kg/m^3	2655	2600
solids average size, μm	200	450

Table 4. Proximate and Ultimate Analyses and Heating Values of the Biomass Used in the Reference Plants

	CFB boiler	BFB boiler
proximate analysis		
moisture, wt %	54.00	40.00
volatiles, wt %	32.00	47.00
char, wt %	13.60	12.60
ash, wt %	0.40	0.40
ultimate analysis (values in wt %)		
C	50.60	
H	5.90	
O	43.20	
N	0.08	
S	0.04	
HHV (dry, ash-free), MJ/kg	17.0−18.5	17.9

5. RESULTS AND DISCUSSION

This section covers (i) the calibration and validation of the model against large-scale measurements, including an analysis of the operational data for the reference boilers under off-design (partial load) operation and (ii) the investigation of the inherent dynamic behaviors of the reference boilers when subjected to changes in load and fuel quality.

It should be noted that combustion in FB units entails inherent variations attributable to the actions taken to control the solids inventory (continuous addition of fuel ash and escape of fly ash, combined with discrete bottom ash discharges and/or additions of makeup solids) impacting on the average solids size and the riser pressure drop—or the variation in the feedstock composition—moisture and volatile content—due to fuel storage. Thus, steady-state operation is here defined as operation during which the operational variables are kept constant for a period of at least 30 min and in which the variability of the process variables lies within ±3%. The measured data utilized in this work have a temporal resolution of 1 every 60 s.

5.1. Model Calibration and Validation. *5.1.1. Steady-State Calibration, Validation, and Analysis.* Calibration of the model is carried out in order to fit the measured operational data from the reference units. Through calibration, specific complex phenomena for which the available knowledge is scarce (here, related to the presence of fines in the freeboard of BFB furnaces due to attrition and the gas mixing) are taken into account through simplified descriptions that are adjusted with unit-specific measurements. Note, however, that the semi-empirical expressions that constitute the model were obtained in units other than the ones modeled here, such as cold flow models and industrial furnaces of wide size range.

For the CFB mode, the model is calibrated by means of the bulk solids size (set to 350 μm) and by adjusting the gas mixing through the effective reaction rate of the homogeneous reactions (see Table 2 and eqs 19−21) in each one of the cells.

https://dx.doi.org/10.1021/acs.iecr.0c06278
Ind. Eng. Chem. Res. 2021, 60, 3936−3956

The calibration is carried out by fitting the measurements obtained from two runs conducted at full load during operation with different levels of fuel moisture and heating values. Although the fitting of the effective rate coefficients reveals a dependency on height, the same values for all reactions can be used, indicating that mixing rather than kinetics governs the homogeneous reactions.

For the BFB mode, the model is calibrated by means of both the gas mixing (similarly to the CFB mode) and the absorptivity in the freeboard. The calibration of the gas mixing through an effective reaction rate coefficient is carried out against operational data obtained at full load. Note that this is unit-specific and, therefore, the calibration factors used differ from those in the CFB unit. The freeboard absorptivity is directly related to the concentration of fines, which strongly depends on the gas velocity/load. Thus, the calibration of absorptivity is fitted to the operational data at two different loads, as shown in Figure 5, where the data indicate that the

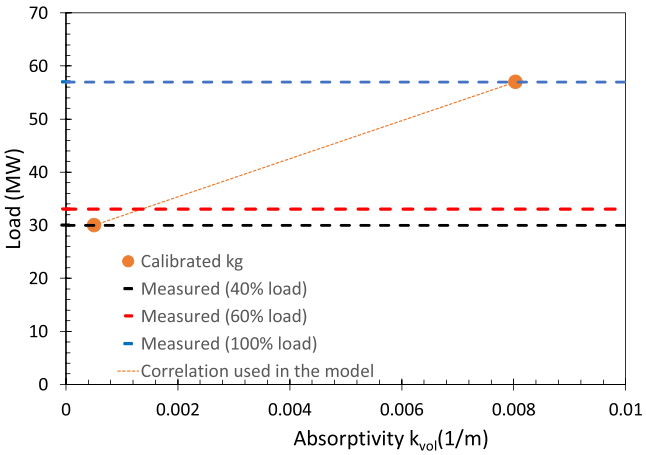

Figure 5. Calibrated absorptivity in the BFB freeboard as a function of the furnace load.

increased presence of fines (resulting from attrition in the freeboard as the load is increased) yields a significant increase in the absorptivity (and thereby on the heat transferred to the walls) from 0.008 1/m at 100% load to 0.0005 1/m at 40% load.

Validation of the steady-state conditions involved two further cases for the CFB unit (at 75 and 50% loads) and one (60% load) for the BFB unit. Note that the data from these validation cases were not used for the calibration, and that the validation cases presented in this section represent a blind validation and not a check of an implicit previous fitting. The calibration and validation results for the relevant process variables are reported in Table 5 in the form of absolute percentage (AP) error (%). The model is shown to be capable of predicting the measured values with a reasonable level of agreement, with all the APs being under 10% and with mean values of 1.9% for the calibration cases and 4.7% for the validation case. Note that for most of the variables, the AP is somewhat higher at lower loads than at full load. Some of the semi-empirical expressions used to formulate the model were obtained for a full-load situation, and some of the model assumptions become less realistic at lower loads (e.g., perfect vertical mixing of the fuel in the dense bed). It is important to mention that the largest errors observed correspond to the gas composition, which to some extent is caused by the fact that the furnaces are modeled through a limited number of cells. Figure 6 presents a parity plot with the calibration and validation results for the heat extracted through the furnace walls.

Figure 7 shows the comparison of the measured and modeled CFB temperature profiles at different loads, including both the calibration and validation cases. Figure 7a reports the data with 18.1 MJ/kg_{daf} wood chips as the fuel, and the data in Figure 7b represent the use of wood chips with 17.1 MJ/kg_{daf}. The temperature profiles throughout the BFB unit are not included due to insufficient measured data points along the combustor.

The above results show the high-level reliability of the model in predicting the steady-state operation at different loads and for the different FB furnace types.

The gas velocity in the furnace, which relates linearly to the boiler load, has a strong impact on the distribution of solids in the furnace. Lower loads yield less solid entrainment from the dense bed into the freeboard and, therefore, lower solid concentrations. This translates into decreased heat transfer to the furnace walls and, as presented in Figure 8, reduced external recirculation of solids. Another consequence of the reduction in load/gas velocity is that the char and volatiles increase their residence times in the bottom part of the furnace, thereby increasing the conversion rate and relative heat release in this region, which leads to a reduction of the temperature in the upper furnace (although this aspect depends on the fuel composition). Furthermore, the lower concentration of solids in the upper freeboard creates a decrease in the local thermal inertia, which makes the temperature in the top region more sensitive to changes (see Table 5). These mechanisms explain the variations in the shape of the temperature profiles observed in Figure 7.

Table 6 shows the computed heat capacities at different loads for the bottom and top regions of the two studied furnaces. It is clear that the heat capacity is strongly linked to the solid concentration, being higher at the dense bed and lower at the top freeboard. In the CFB furnace, the breakdown of the contributions of each phase to the total heat capacity varies across the regions, being in the ranges of 5−10% for the fuel, 1−10% for the gas, and 80−90% for the bulk solids. As discussed above, the solid entrainment is reduced at lower loads, yielding a displacement of solid mass from the top to the bottom, which is reflected in terms of the heat capacity. On the contrary, in the BFB furnace, the heat capacity remains approximately constant in both regions when the load is changed, since the model does not account for solids entrained from the dense bed, showing a slight decrease in heat capacity at lower loads due to the reduced fuel inventory.

5.1.2. Transient Operation Validation and Discussion. Measurements made during load changes are used for validating the model under transient conditions. For the reference CFB unit, an increase in load from 50 to 100% in 180 min is studied. The transient values for the main operating conditions are given in Figure 9a. The measured data had a time resolution of 1 min and, thus, was linearly interpolated into a shorter time scale (1 s), in order to serve as an input to the model. Modeled output data are compared to the measurements: heat transferred to the walls (Figure 9b) and temperatures in the furnace (at a height of 6 m; Figure 9c) and cyclone (Figure 9d). The model is found to predict successfully the trajectories of these main process variables, showing especially good agreement for the heat transferred to

https://dx.doi.org/10.1021/acs.iecr.0c06278
Ind. Eng. Chem. Res. 2021, 60, 3936−3956

Table 5. Steady-State Results for the Model Calibration and Validation (Results Are Shown as Absolute Percentages (AP) Error (%), and Absolute Values)

	CFB boiler				BFB boiler		
	calibration		validation		calibration		validation
variable	100% load 1	100% load 2	75% load	50% load	100% load	40% load	60% load
Q_{wall} [MW]							
measured	45.00	45.00	31.30	23.0	56.20	28.00	30
modeled	46.90	43.70	33.50	23.85	57.80	29.00	31.20
AP (%)	4.22	2.89	7.03	3.70	2.85	3.57	3.33
T_{top} (°C)							
measured	862	845	830	713	935	794	822
modeled	856	830	845	740	948	819	819
AP (%)	0.70	1.78	1.81	3.79	1.39	3.15	0.36
$T_{cyclone}$ (°C)							
measured	880	862	846	726			
modeled	878	860	851	741			
AP (%)	0.22	0.23	0.59	2.07			
T_{db} (°C)							
measured	796	759	778	750	820	817	814
modeled	797	760	783	725	830	780	800
AP (%)	0.13	0.10	0.64	3.33	1.22	4.53	1.72
X_{CO2} (%v)							
measured	16.30	14.70	16.30	12.80	12.77	11.20	13
modeled	15.70	15.40	15.30	13.80	13.00	12.10	14
AP (%)	3.68	4.76	6.13	7.81	1.80	7.14	7.69
X_{O2} (%v)							
measured	2.00	2.60	2.00	3.20	2.70	2.70	3.00
modeled	2.10	2.65	2.17	3.00	2.70	2.95	2.90
AP (%)	5.00	1.92	8.50	6.25	0.00	9.26	3.33

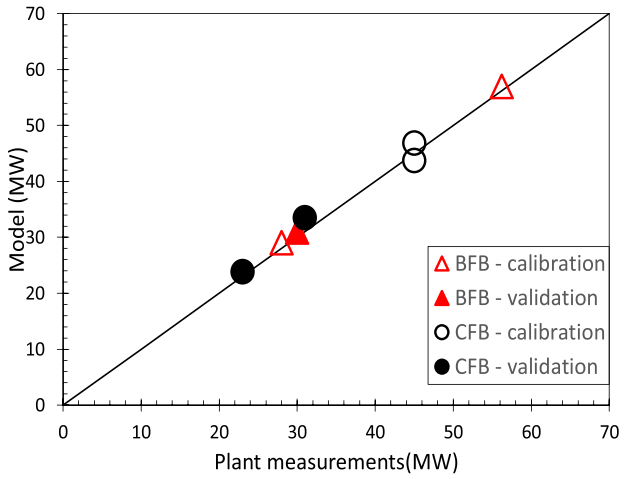

Figure 6. Parity plot for the total heat transferred to the walls for the seven steady-state operation cases.

the walls. Note that Figure 9c shows drops in the measured temperature whenever the secondary air injection is sharply increased. This is not captured by the model because this effect is believed to be due to a local cooling phenomenon around the measurement instrument rather than effective cooling of the entire volume represented by the corresponding cell.

For the reference BFB unit, a load increase from 56 to 90% in 130 min is studied. The dynamics of the inlet boundary conditions are plotted in Figure 10a. The three output variables monitored are the total heat transferred to the walls (Figure 10b), the temperature in the dense bed (Figure 10c), and the temperature before the superheaters (i.e., at a height of 10 m; Figure 10d). Similar to the CFB unit, the model of the BFB unit shows good agreement when predicting the trajectories over time, especially for the total heat transferred to the walls. Note that the plotted dense bed temperature measurement reflects the average of the measurements collected by the nine instruments located in the region, which may explain why the modeled and measured trajectories differ slightly more than other variables.

It is worth mentioning that the present dynamic validation approach does not cover the short time scales for the fast gas flow dynamics inherent to FB furnaces, since industrial units in current Nordic energy systems apply load changes at relatively slow ramping rates (e.g., the above cases with 0.2 MW/min for CFB and 0.4 MW/min for BFB). In order to validate the inherent dynamics of the in-furnace combustion process, measurements under open-loop tests are needed. However, such tests cannot be carried out in commercial installations due to safety and operational constraints. Nevertheless, it can be concluded from Figures 9 and 10 that the dynamic model presented in this work successfully predicts the trajectories of the main process variables during transient operation at ramping rates typical for industrial furnaces.

Several studies in the literature dealing with dynamic modeling of FB conversion ([14−16,58]) have, for simplicity, assumed a static mass balance (the mass in any cell does not vary with time) when formulating the dynamic energy balance to solve the transient temperature and heat extraction. Equation 32 shows the general derivation of the accumulation term in the energy balance, which results in a mass variation term and a temperature variation term, representing the full energy balance (full EB) applied in this work. The mass variation term is, however, ignored in the simplified energy

https://dx.doi.org/10.1021/acs.iecr.0c06278
Ind. Eng. Chem. Res. 2021, 60, 3936−3956

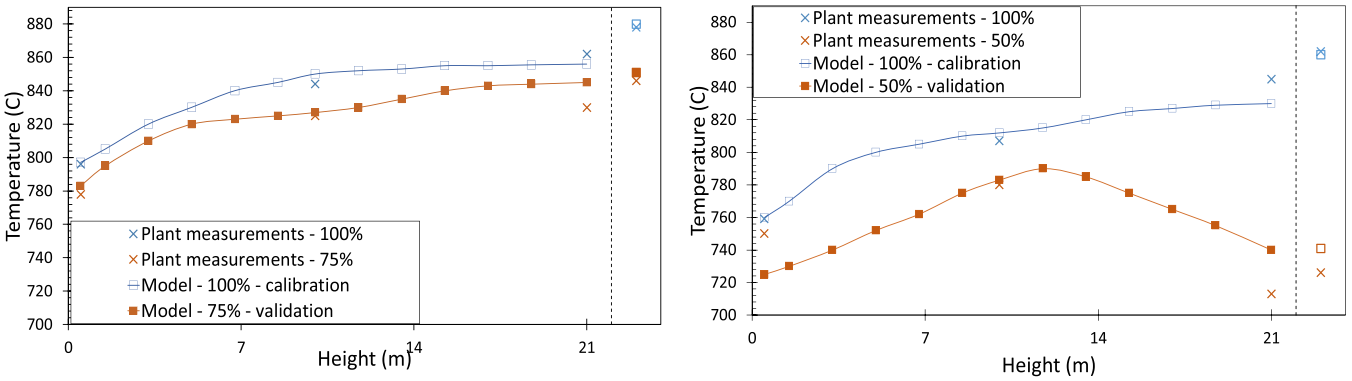

Figure 7. Simulated and measured temperature points in the CFB reference furnace for two different operational periods. The points added to the right of the profiles represent the cyclone temperatures.

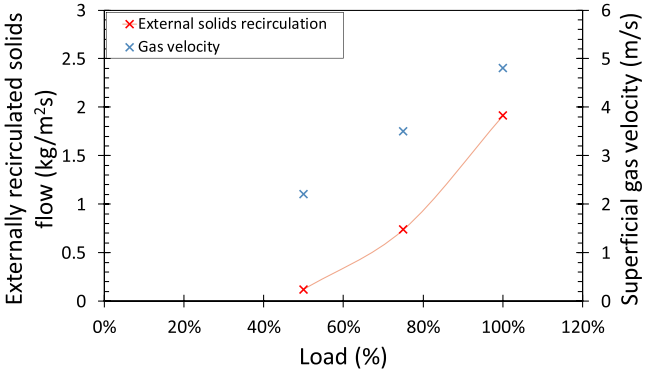

Figure 8. Simulated external solids circulation in the CFB reference furnace for different loads/superficial gas velocities.

Table 6. Heat Capacities of the Bottom and Top Regions in the CFB and BFB Furnaces under Different Loads

heat capacity [MJ/K]		maximum load	medium load	minimum load
dense bed	CFB	24.0	27.3	29.3
	BFB	35.7	35.3	35.1
freeboard top	CFB	0.28	0.14	0.05
	BFB	0.07	0.07	0.06

balance (simplified EB) approach that assumes a static mass balance, following the classical derivation in single-phase flow reactors.

$$\frac{dE}{dt} = \frac{d(mh)}{dt} = m\frac{dh}{dt} + h\frac{dm}{dt} = (h_0 + C_p(T - T_{ref}))\frac{dm}{dt} + mC_p\frac{dT}{dt} \quad (32)$$

Figure 11 illustrates the trajectory of the temperature at the furnace top when a −25% step-change in the load is simulated, while accounting for or neglecting the mass variation term. A strong impact of the furnace top temperature is observed for the CFB case but not for the BFB case. This can be explained by the significant mass transfer that occurs between regions in the CFB as the load is changed, while BFB units retain all the solids (and, thereby, most of the system's mass) in the same region—the dense bed. Disregarding the mass variation term (first term of the right-hand-side of eq 32) causes strong fluctuations (up to 30% of the steady-state value) in the modeled temperature during the first seconds of the transient. These effects gradually disappear when the ramping rate is smoothed (see discussion on the variable ramping rate in Section 5.2.1). This would justify the use of the assumption of a static mass balance in studies that aim to simulate slow process changes (e.g., typical industrial operation and/or the dynamics of the water side). The assumption is also justified in cases where the process is rapid but the mass in each cell does not change significantly, e.g., disturbances such as fuel shifts and fuel line stops, or when the energy balance is applied as a single zero-dimensional balance to the entire furnace, assuming no change in the total mass. Thus, it can be stated that the formulation of the full EB is necessary for an accurate description of the inherent dynamics of CFB furnaces that are discretized into several control volumes.

5.2. Open-Loop Dynamic Analysis. The aim of this section is to characterize the open-loop, i.e., in the absence of any control, dynamic responses of commercial-scale FB units to different load changes, and fuel variations, and to identify the characteristic time-scales for these responses at the reactive side. Data obtained from simulations with the validated model are used for these analyses, as commercial operation is strongly controlled and does not allow one to study the inherent responses of the reactive side to operational changes.

5.2.1. Load Change. This subsection investigates the open-loop responses to load changes, including the effects of the change magnitude and rate as well as of the thermal inertia in the system (i.e., the amount of solids).

First, the dynamic performances of the reference furnaces after a step reduction in load from 100 to 75% (Figure 12a) are investigated. For this, simultaneous step changes from nominal values to 75% load are introduced for different model inputs: air and fuel flows and heat extracted by the superheaters immersed in the furnaces. The responses of the main process variables for the CFB and BFB furnaces are shown in Figure 12b–f (note the different scale of the x-axes for each type of unit).

The load decrease eventually drives both unit types to a new steady state, with obviously lower furnace temperatures and heat extraction. In the CFB furnace, the bottom temperature is reduced to a lesser extent than the top temperature (see Figure 12b), caused mainly by the fact that the sudden decrease in gas velocity quickly increases the mass of solids in the dense bed,

https://dx.doi.org/10.1021/acs.iecr.0c06278
Ind. Eng. Chem. Res. 2021, 60, 3936−3956

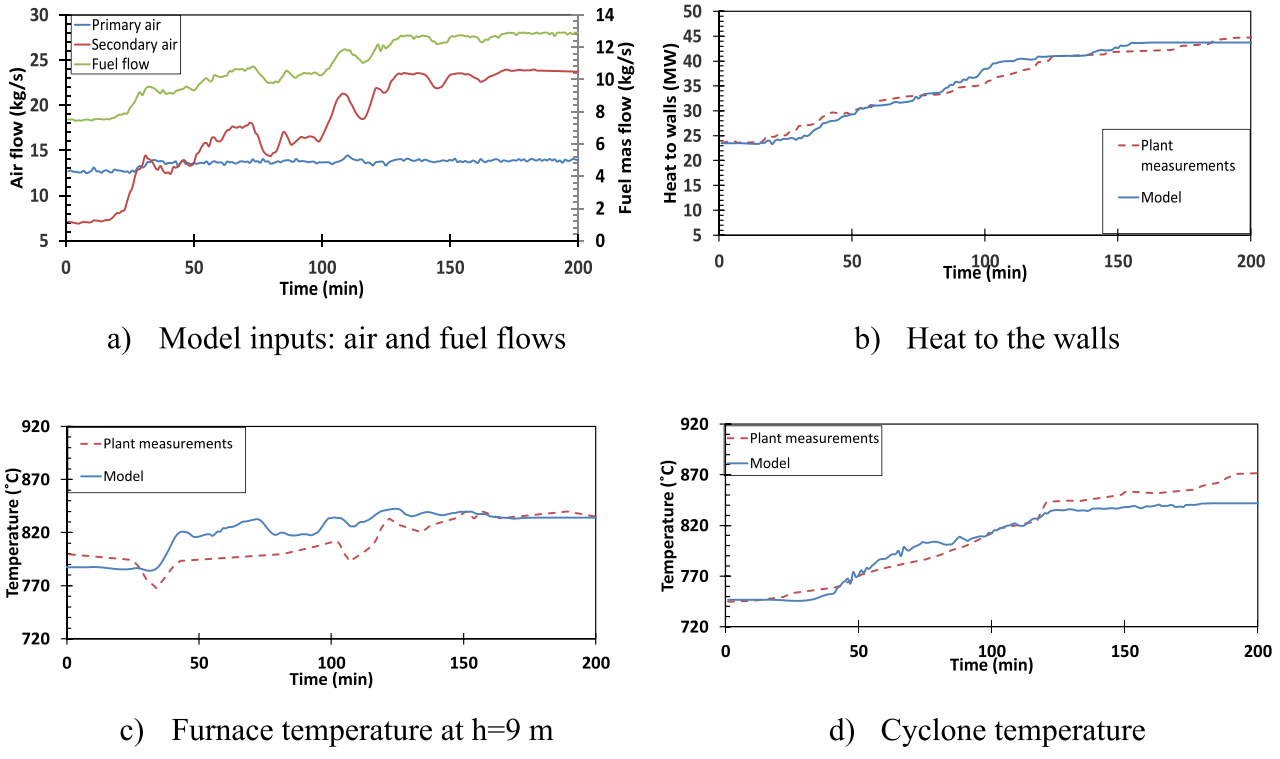

a) Model inputs: air and fuel flows

b) Heat to the walls

c) Furnace temperature at h=9 m

d) Cyclone temperature

Figure 9. Model validation for a load change from 50 to 100% in the CFB unit.

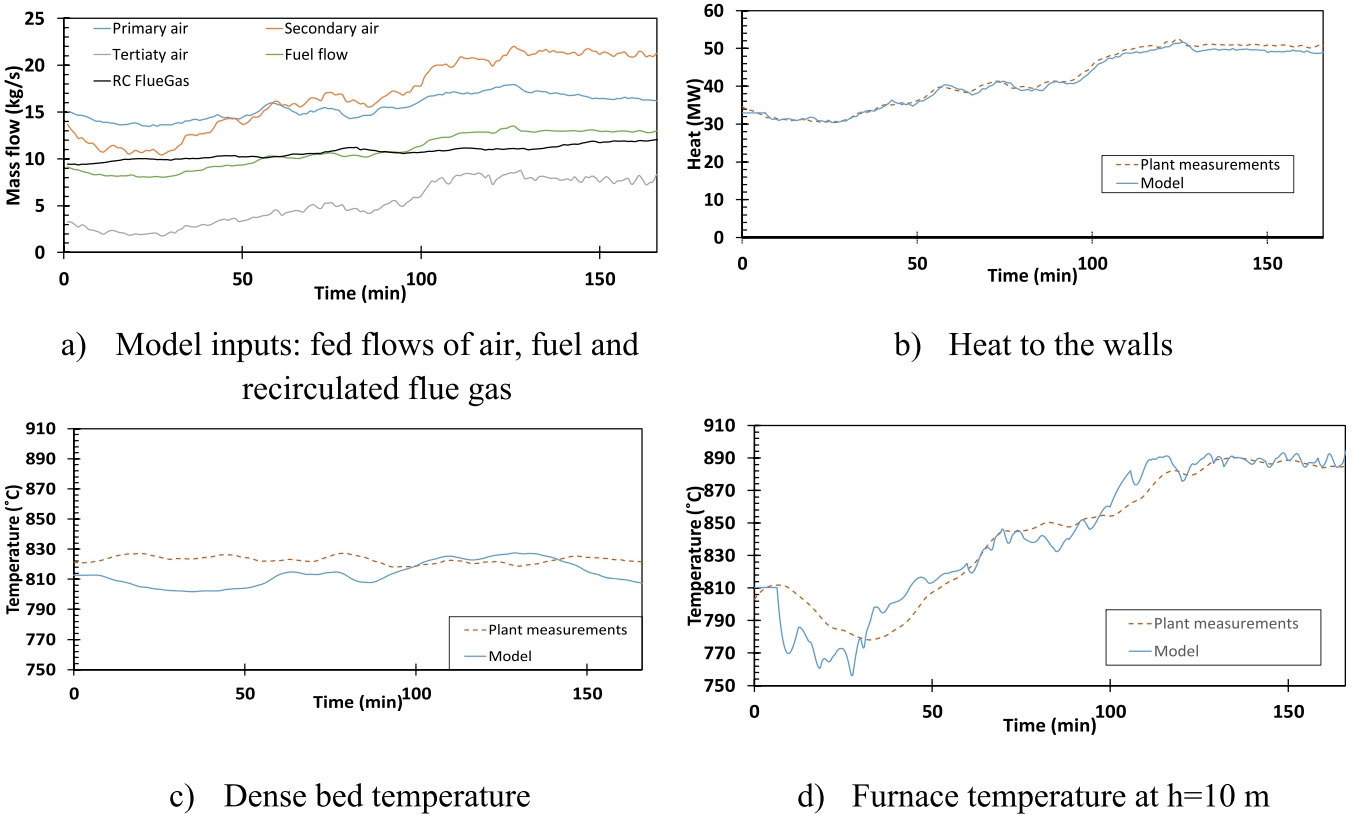

a) Model inputs: fed flows of air, fuel and recirculated flue gas

b) Heat to the walls

c) Dense bed temperature

d) Furnace temperature at h=10 m

Figure 10. Model validation for a load change from 56 to 90% in the BFB unit.

including char (see Figure 12d), despite the reduced fuel feeding. This is in line with the model results in a previous study[23] simulating step-changes in a 0.3 MW unit. Due to the large thermal inertia of the dense bed, the temperature transient evolves smoothly toward the new steady state. Furthermore, the dense bed temperature is strongly affected by the recirculation of solids, which has an inherent delay due to the residence time in the circulation loop (in this case, about

https://dx.doi.org/10.1021/acs.iecr.0c06278
Ind. Eng. Chem. Res. 2021, 60, 3936−3956

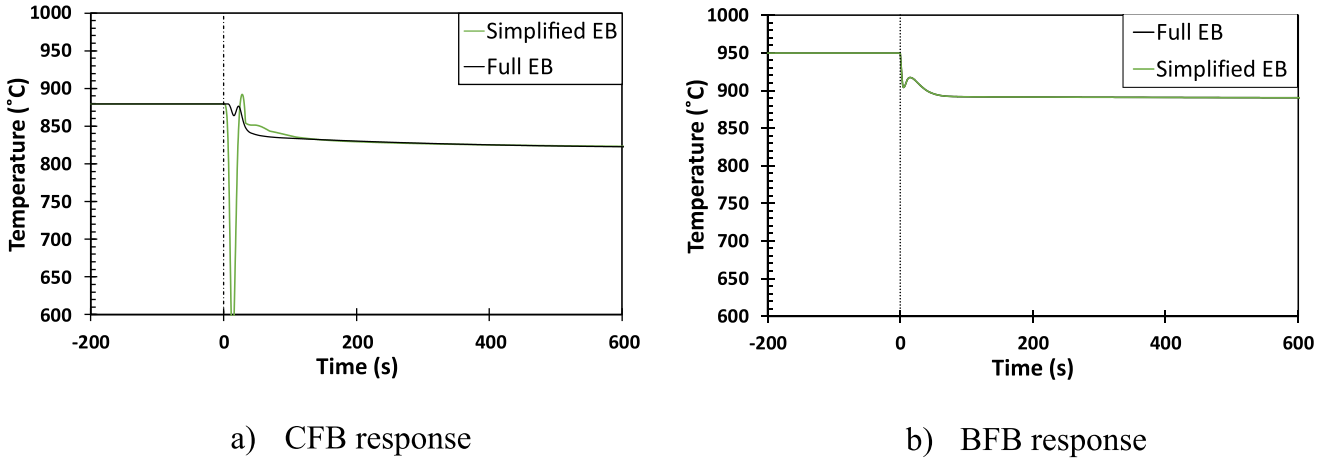

Figure 11. Open-loop trajectories of the top furnace temperature for a 25% decrease in load when the energy balance accounts for (full EB) or disregards (simplified EB) the dynamics in the mass balance.

30 s). The top of the furnace, in contrast to the bottom, exhibits abrupt variations in temperature at the very beginning of the transient, caused by the low heat capacity of the region (with a low solids concentration), in combination with momentary significant differences in the heat flows conveyed in and out of the region by the solids flows, as illustrated in Figure 12d as the net energy flow carried by the solids at the furnace top, $H_{net,top}$. Regarding heat extraction, Figure 12f shows the convective and radiative heat transferred to the walls from a control volume located in the upper furnace. As the solid concentration suddenly drops due to the reduction in load, the convective heat also decreases precipitously, while the radiative contribution increases (albeit to a minor extent), which explains the rapid initial decrease in total heat extraction (see Figure 12b). It is evident that both heat transfer mechanisms undergo a sudden response (related to the solids concentration) followed by a slower one (related to the temperature, which is of greater significance for the radiation of heat). The last part of the heat extraction transient follows closely the temperature of the core region in the upper furnace, since radiation becomes the driving mechanism at the established lower load level.

When it comes to the dynamics of the BFB furnace, Figure 12c shows that T_{db} follows a similar trajectory to that in the CFB unit, characterized by a slow transient due to the large heat capacity and a low oxygen concentration in the region, yielding a slower combustion rate that is mainly due to decreased combustion of volatiles (the decrease in char inventory is only moderate), as presented in Figure 12e. In contrast, the temperature in the furnace visualized as T_{top} in Figure 12c experiences a rapid drop due to the sudden reduction in gas emissivity followed by a somewhat slower transient that is driven by the combustion of volatiles and the delay associated with the flue gas recirculation, as illustrated in Figure 12e. This fast response drives the transient of the heat transferred to the walls, which is mostly affected by the gas temperature and gas emissivity.

The effect of the magnitude of the load change is studied through load step-changes of −10, −20, and −50%, respectively, starting at full load (Figure 13a). As expected, most of the variables show increased relative changes for more extensive load changes. The obtained stabilization times (the time required to overcome 90% of the total change) and the relative changes of the main process outputs (Figure 13b−e) indicate that regions with higher concentrations of solids (the furnace bottom) exhibit smaller relative changes and longer stabilization times and vice versa. Consequently, the difference in stabilization time between the bottom and top furnace temperatures is much larger for the BFB furnace (∼20 min and a few seconds, respectively), as it contains a denser bottom region and a solid-free furnace top, as compared to the CFB furnace (∼10 and ∼5 min, respectively). As a direct function of temperature, the extracted heat follows the same pattern. In general, the CFB case shows longer stabilization times for the dense bed temperature and heat extraction as the magnitude of the load change is increased, while the results for the BFB case are not as conclusive.

When simulating a 25% step-up in load from 75 to 100%, the trend of slower stabilization for regions with high concentrations of solids is retained. However, significantly shorter stabilization times with respect to the step-down between the same load levels are observed in both units (see Figure 13b,d). This effect is typically observed in thermal processes and reflects the fact that increasing the temperature of a system tends to be faster due to the presence of a heat source driving the process, whereas reducing the temperature relies on cooling through a temperature difference with the surrounding temperature.

While the step-response analysis described above gives insights into the inherent dynamics of the reactors, a variable ramping rate analysis is performed to study the responses under conditions approaching those typical for industrial operation. Figure 14a shows the three cases simulated, applying a load reduction from 100 to 75% at ramping rates with characteristic times of 0 (step change), 60, and 600 s, respectively. Note that these ramping rates are still faster than those of the experimental industrial cases shown above (see Figures 9 and 10), with an approximated ramping rate of 25%/5500 s, due to the fact that in some scenarios, e.g., in the Nordic countries, FB combustors are driven by the dispatchability within the district heating network and are therefore subjected to slower load changes than those boilers that follow the electricity demand.[59] The responses plotted in Figure 14b (CFB unit) and Figure 14c (BFB unit) show that the inherent system dynamics observed in the open-loop trajectories disappear for the slowest ramping rate. This means that the system is fast enough to adopt a pseudo-steady-state behavior, i.e., at any time during load ramping, the system

https://dx.doi.org/10.1021/acs.iecr.0c06278
Ind. Eng. Chem. Res. 2021, 60, 3936−3956

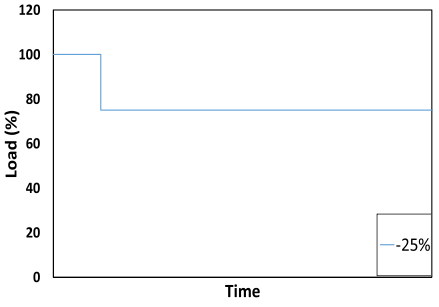

a) Simulation of a -25% step-change in the load simulated

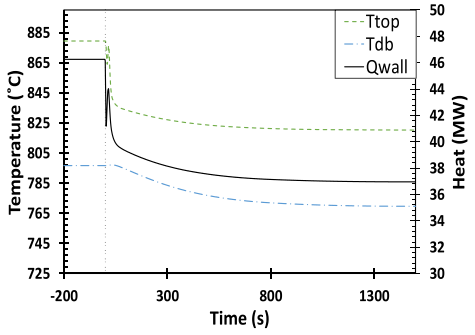

b) Open-loop responses of T_{db}, T_{top} and Q_{wall} in the reference CFB furnace.

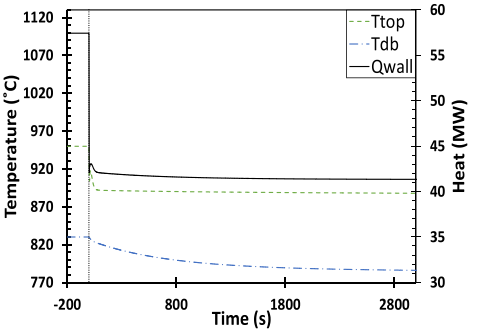

c) Open-loop responses of T_{db}, T_{top} and Q_{wall} in the reference BFB furnace.

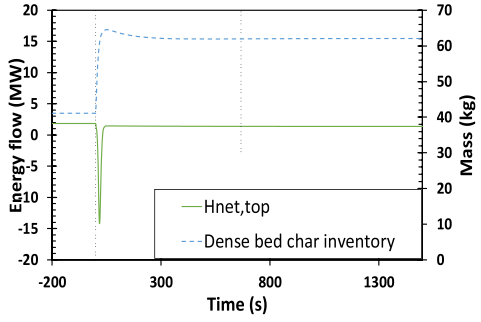

d) CFB responses of the net energy flow carried by the solids in a cell at the furnace top and the char inventory in the dense bed.

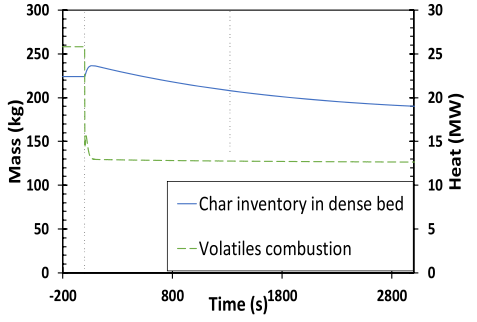

e) BFB responses of the char inventory in the dense bed and the heat released by the combustion of volatiles in a certain cell of the upper furnace.

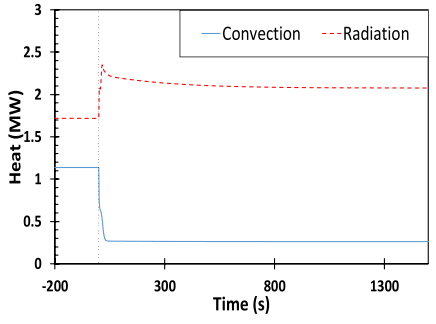

f) CFB responses for convective and radiative heat flows into the walls of a certain cell of the upper furnace.

Figure 12. Open-loop responses of the CFB (b, d, f) and BFB (c, e) reference furnaces when a −25% load change (a) is simulated at $t = 0$, represented by the vertical dashed line.

parameters adopt the same values that they would have in the steady state. Generally, process variables with an open-loop settling time shorter than the rate of change introduced will display a pseudo-static response. Thus, variables with faster

https://dx.doi.org/10.1021/acs.iecr.0c06278
Ind. Eng. Chem. Res. 2021, 60, 3936−3956

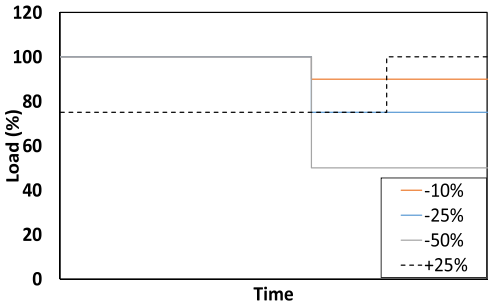

a) Step-changes used for studying the effect of the load change magnitude.

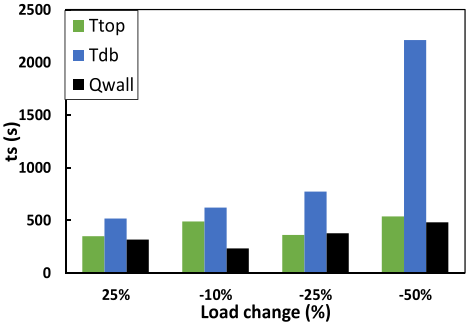

b) CFB stabilization times for different load changes.

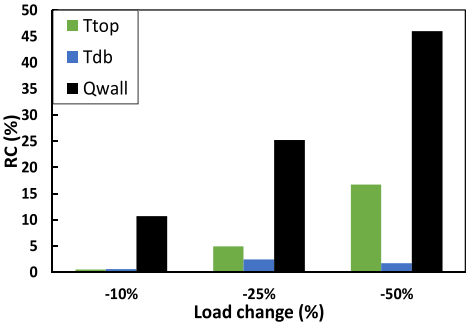

c) CFB relative changes for different load changes.

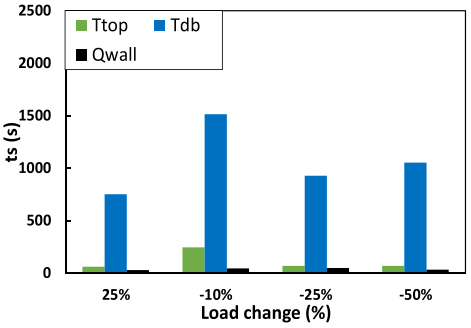

d) BFB stabilization times for different load changes.

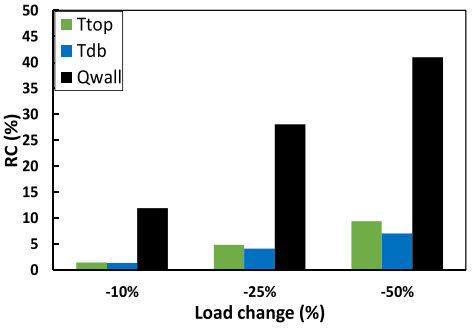

e) BFB relative changes for different load changes.

Figure 13. Stabilization times t_s (s) and relative changes RC (%) of the main process variables of the CFB and BFB units when load changes of different magnitudes are simulated. Note that the RC of the +25% load change is the same as for the −25% load change, so it has not been included here.

responses (such as the temperature at the BFB furnace top, with $t_{s,100\rightarrow75\%}$ = 60 s; see Figure 13d) tend to follow more closely the load change (especially the slow ones) and exhibit different behaviors as the disturbance is slowed and some of the dynamics are hindered, i.e., those related to processes with characteristic times shorter than the perturbation ramping rate (see Table 7). Instead, for slow-response variables (such as the BFB dense bed temperature, with $t_{s,100\rightarrow75\%}$ = 900 s; see Figure 13d), the responses to the load change are still not settled after the new load is reached. These aspects take on particular importance when one considers industrial operation, particularly in future energy systems in which these furnaces will be pushed to adapt quickly to changes on the demand side. Fast load changes can lead to peaking emissions (for which the regulations are increasingly restrictive[60]), as depicted in Figure 14d as the overshoot in CO emissions during a load change at different ramping rates in the BFB furnace. It can be seen that the sudden temperature drop caused by the step change leads to large peaks of unburnt CO, whereas slower ramping reduces this effect.

Operation of FB boilers involves batch removals and/or additions of bed material from/to the system. These result in variations to the solid inventory in the furnace, which can extend to ±40% of the nominal values. Figure 15 shows the results of a −25% load change in the BFB unit with different solid inventories (limited to ±10% of the nominal value for simplicity). A rather strong impact is observed on the stabilization time of the dense bed temperature, varying by up to 15%, while that of the total heat transferred to the walls is hardly affected (being the latest mostly driven by the upper furnace temperature and gas emissivity, as discussed above).

https://dx.doi.org/10.1021/acs.iecr.0c06278
Ind. Eng. Chem. Res. 2021, 60, 3936−3956

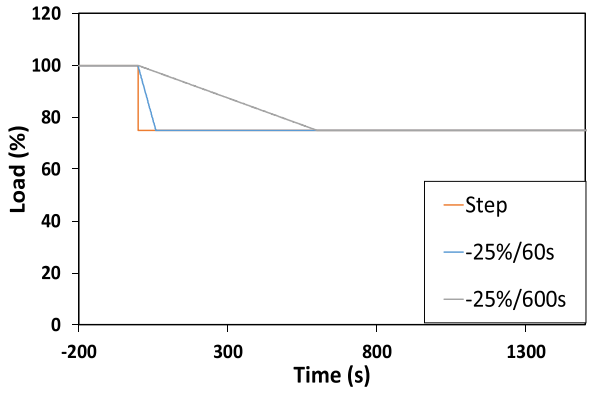

a) Variable ramping rate analysis.

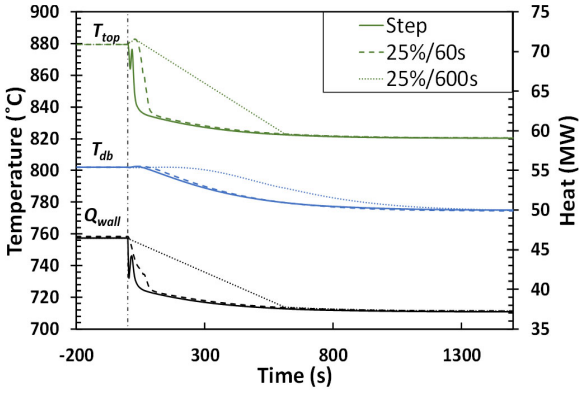

b) CFB responses of T_{db}, T_{top} and Q_{wall} to different ramping rates.

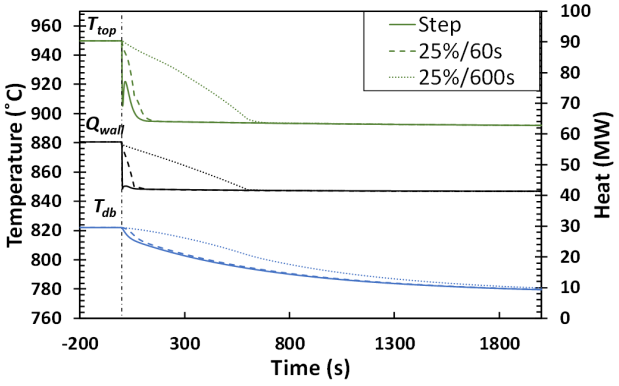

c) BFB responses of T_{db}, T_{top} and Q_{wall} to different ramping rates.

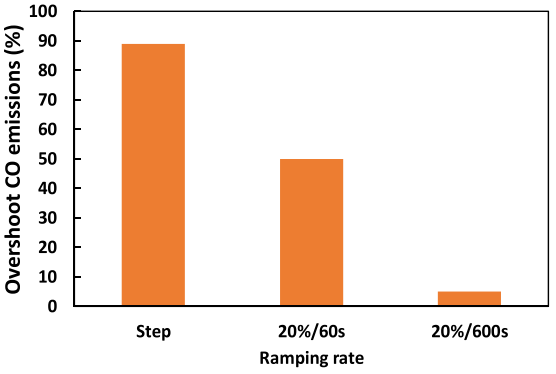

d) Overshoot of CO emissions in BFB unit when the load is changed at different ramping rates.

Figure 14. Variable ramping rate analyses. (a) Input ramping rates, (b) CFB results for T_{top} and Q_{wall}, (c) BFB results for T_{db} and T_{top}, and (d) overshoot (%) of CO emissions in the BFB unit.

Table 7. Characteristic Time Constants of the Three Major In-Furnace Mechanisms

mechanism	characteristic time τ	value (seconds)
fluid dynamics	$\tau = \frac{H}{(u-u_t)} + \frac{H}{u_t}$ or $\tau = \frac{H}{u}$	15−30
heat transfer	$\tau = \frac{m_{\text{furnace}} \times C_p \times \Delta T}{\dot{Q}_{\text{in,furnace}}}$	150
fuel conversion	$\tau = t_{\text{dry + dev}}$	50

5.2.2. Changes in Fuel Moisture Content. This section investigates the inherent dynamics of the reference furnaces when a sudden change in fuel moisture (±5%) occurs while the furnaces are running at 100% or 75% load. Focusing on the inherent dynamics, the furnaces are not controlled, i.e., the inflows of air and fuel are kept constant.

The modeled stabilization times of the main process variables after the ±5% step changes in fuel moisture content are summarized in Figure 16. They show that both the BFB and CFB boilers respond faster to the moisture change when operated at full load. The reason for this is that higher loads imply higher gas velocities and, therefore, shorter gas residence times. The exception to this trend is found in the BFB dense bed temperature, which is explained by a reduction of the fuel inventory and its corresponding heat capacity. Another aspect that is inferred from Figure 16 is that the systems respond faster when the moisture content is decreased (and thus the furnace temperature is increased) rather than increased. This is in line with the previous observation that load increases

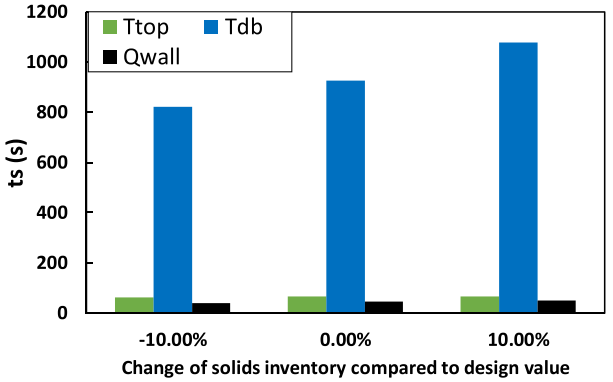

Figure 15. Effects of ±10% changes in the solid inventory of the BFB unit on the stabilization time t_s (s) for a −25% load change.

https://dx.doi.org/10.1021/acs.iecr.0c06278
Ind. Eng. Chem. Res. 2021, 60, 3936−3956

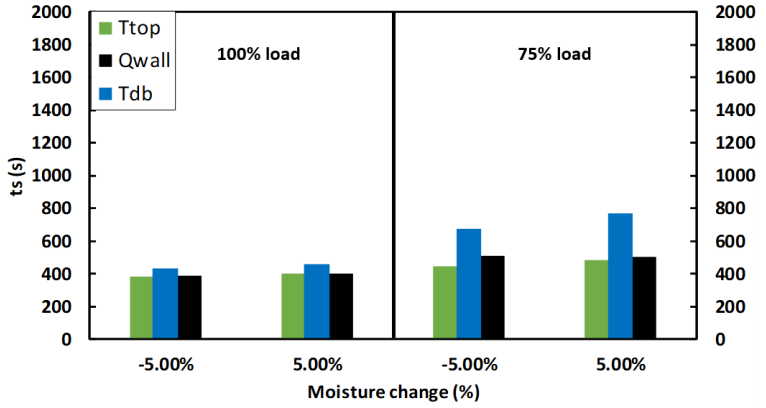

a) Stabilization times of the CFB variables for step-changes in moisture content of the fuel.

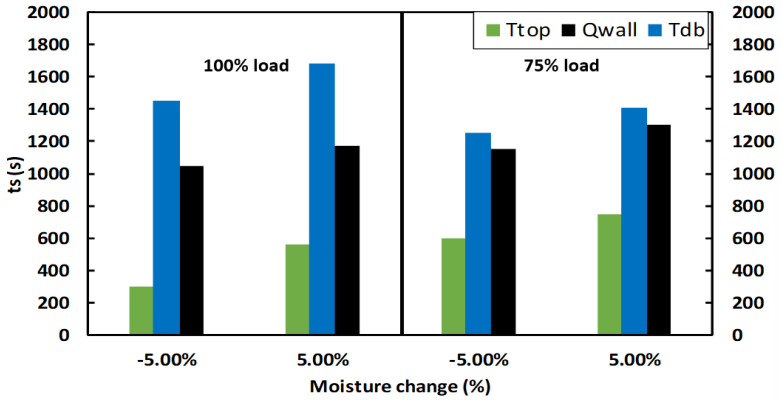

b) Stabilization times of the BFB variables for step-changes in moisture content of the fuel.

Figure 16. Stabilization times t_s (s) for a moisture change of ±5% when the furnaces are running at 100 and 75% loads for the (a) CFB furnace and (b) BFB furnace.

stabilize faster than load reductions (see Figure 13 and corresponding discussion). Note that the dense bed is once again the last region to reach steady state, owing to its large heat capacity (as discussed above), in addition to the fact that in both boilers, most of the drying (all of it in the BFB unit) occurs in the dense bed.

5.2.3. Final Remarks. As a general analysis tool to assess the dynamic behavior of FB furnaces, the characteristic times of the three main process mechanisms in the furnace—fluid dynamics, fuel conversion, and heat transfer—are estimated in Table 7. Regarding the fluid dynamics, the characteristic time is estimated as the time that it takes for the solids to flow up the riser plus the time that it takes for the solids to be recirculated. Since it is the case in CFB furnaces that the vast majority of the solids are internally recirculated, the internal recirculation time is considered. For BFB furnaces, the residence time of the gas in the furnace is taken instead. The characteristic time of fuel conversion is taken as the time required for drying and devolatilization, with moisture and volatiles comprising most of the content of biomass and other low-rank fuels. It is seen that the slowest mechanism is the heat transfer, due to the large thermal inertia of the furnace, whereas the fluid dynamics and the fuel conversion rates are much faster. This is in agreement with the transient responses illustrated in Figure 12b,c, where the abrupt variations observed in T_{top} and Q_{wall} occur within the first 20 s, i.e., while the solids flows are varying. The estimated characteristic times can also aid the understanding of the different behaviors observed when increasing and decreasing the load, i.e., a load increase is driven by the fuel conversion, whereas the heat transfer to the walls drives a load reduction, with the latter always being slower, as shown in Figure 13.

Several implications can be drawn from the dynamic analysis described above. Regarding stabilization times, Table 8 summarizes the settling times of the main process variables considered in this work under the investigated changes in conditions. The outcome represents valuable information for future studies characterizing the dynamics of an entire power plant, i.e., accounting for the water−steam equipment. The

Table 8. Stabilization Times (in Minutes) of the Process Variables Included in the Open-Loop Dynamics Analysis for the Load and Fuel Changes Investigated

	CFB unit	BFB unit
T_{db}	6−36	12−27
T_{top}	5−9	1−12
Q_{wall}	3−8	0.4−18

https://dx.doi.org/10.1021/acs.iecr.0c06278
Ind. Eng. Chem. Res. 2021, 60, 3936−3956

results of the present study can also serve as inputs for investigations related to the testing and comparison of different furnace control strategies, although further studies, such as detailed analyses of the interactions between variables, are required.

The simulations show that the furnaces can maintain stable operation under rapid transient changes of temperature and heat transfer, although some undesired peaking emissions of unburnt matter. According to the EU Emissions Directive,[60] for these types of boilers, the emissions of CO must be continuously monitored and the daily average should not be >110% of the emissions limit. It is foreseen that fast ramping rates will be pursued in future energy systems in which increased flexibility with regard to the dispatchability of thermal plants will be required. Thus, the results extracted from the present work may be of importance when analyzing further the flexibility capabilities of FB boilers. Other aspects need to be considered when assessing the plant possibilities for fast changes, such as the thermal stresses in thick-walled components.[61] The findings presented in this work play a crucial role when analyzing the feasibility of flexible operation of specific FB combustors under different scenarios. For instance, a specific boiler might be operated both flexibly and smoothly under the variation rates seen in heat demand-driven operation (which yield a pseudo-static state operation), whereas the rapid variations typical of electricity-driven operations may manifest stronger inherent dynamics.

The modeling approach presented in this work constitutes a valid description of the dynamics of large-scale fluidized bed combustors. Thus, it could be further integrated into process models of the entire heat and power plant. The model can also be applied to test and compare different control schemes. Furthermore, the model could be retrofitted to account for thermal processes other than conventional combustion, in order to investigate the behaviors of other fluidized bed applications, such as polygeneration reactors, gasifiers, and chemical looping combustors. Another research area that could be expanded from this work is the simplification of the model equations in order to determine key model order reductions based on physical insights or surrogate modeling.

6. CONCLUSIONS

A dynamic model of the reactive side of a large-scale fluidized bed combustor is presented. The modeling procedure consists of calibration, validation, and application under steady-state and transient conditions. The model has been built using a generic formulation and is satisfactorily validated to describe multi-load, steady-state, and transient industrial operation of the reference units chosen (an 80 MW CFB and a 130 MW BFB). The model is calibrated using a restricted set of variables by means of gas mixing, bed material particle size (exclusively for the CFB case), and disperse-phase emissivity at full load (exclusively for the BFB case).

The results of the off-design analysis show that the heat capacity plays a central role in the stabilization times for the temperatures in the different regions. In the CFB furnace, the larger heat capacity of the lower furnace, in comparison to the top locations (a consequence of the difference in solids concentrations), becomes more prominent as the load is decreased, thereby approaching the largest difference represented by the BFB furnace. The present work underlines the importance of accounting for the solids present in the freeboard (namely through gas emissivity) when calculating the radiative heat transfer in BFB units, and it deduces the decreased presence of such solids as the boiler load is reduced.

From the results obtained for the open-loop responses to load and fuel changes, the following are concluded:

(i) For the load changes simulated, the stabilization time of the heat transferred to the furnace waterwalls is in the order of hundreds of seconds in both units, averaging 6 min in the CFB unit and less than 2 min in the BFB unit.

(ii) In FB combustors, the bottom bed exhibits the slowest response of the furnace due to its large heat capacity and low oxygen concentration. The temperatures at the top of the furnace reach stabilization faster, although they are more sensitive to changes in load and fuel. For the CFB unit, the upper part of the furnace stabilizes 1−3 times (5−9 min for stabilization) faster than the bottom bed, whereas for the BFB unit, the freeboard can stabilize up to 10 times faster (1−12 min for stabilization) than the bed.

(iii) When disturbances are introduced into the unit, the dynamics of the process variables with settling times shorter than those characterizing the disturbance are hindered. If one slows down the disturbances to industrial operation values, the processes in the furnaces become quasi-static.

(iv) FB furnaces respond faster to changes when they are running at higher loads due to increased gas velocities.

(v) Given two load levels, FB furnaces reach stabilization faster when the load is increased than when it is decreased, since heat transfer drives the load reduction, whereas fuel conversion drives the load increase.

(vi) In models that discretize the riser, considering the mass balance as static when solving the energy balances is found to yield significant errors for CFB furnaces owing to the large variations in mass caused by the circulating solids. For BFB designs, however, this term can be ignored in the energy balance, i.e., assuming the mass in each region to be static.

Further research to increase the knowledge regarding solid entrainment from the bottom bed and backflow effect at the furnace exit is crucial to enhance the generic accuracy of the model. Additionally, fast load-change tests in industrial units would be needed to validate the open-loop dynamics predicted by the model.

AUTHOR INFORMATION

Corresponding Author

Guillermo Martinez Castilla − *Division of Energy Technology, Chalmers University of Technology, Gothenburg 412 96, Sweden;* orcid.org/0000-0002-0258-3890; Email: castilla@chalmers.se

Authors

Rubén M. Montañés − *Division of Energy Technology, Chalmers University of Technology, Gothenburg 412 96, Sweden; SINTEF Energy Research, Trondheim NO-7465, Norway;* orcid.org/0000-0002-6600-5512

David Pallarès − *Division of Energy Technology, Chalmers University of Technology, Gothenburg 412 96, Sweden*

Filip Johnsson − *Division of Energy Technology, Chalmers University of Technology, Gothenburg 412 96, Sweden*

Complete contact information is available at: https://pubs.acs.org/10.1021/acs.iecr.0c06278

https://dx.doi.org/10.1021/acs.iecr.0c06278
Ind. Eng. Chem. Res. 2021, 60, 3936−3956

Notes

The authors declare no competing financial interest.

■ ACKNOWLEDGMENTS

The authors express their gratitude to the financial support provided by the Swedish Energy Agency (project 46459-1, "Cost-effective and flexible polygeneration units for maximised plant use").

■ NOMENCLATURE

Greek

α absorptivity [m^{-1}]
ε voidage, emissivity
Ω stoichiometry coefficient [2]
ρ density [kg m^{-3}]
σ Stefan−Boltzmann constant [5.6 ×10^{-8} W m^{-2} K^{-4}]
η Efficiency
τ characteristic time [s], residence time, [s]

Latin

A area [m^2]
c specific heat capacity [J kg^{-1} K^{-1}], concentration [kg m^{-3}]
D diameter [m], diffusivity [m^2 s^{-1}]
E energy [J]
F view factor
h specific enthalpy [J kg^{-1}], variable height [m], convective heat transfer coefficient [W m^{-2} K^{-1}]
H total height [m]
k constant, backflow effect coefficient, absorption coefficient
K transport decay factor
L length [m]
m mass flow [kg s^{-1}], mass [kg]
M molar mass [g/mol]
P pressure [bar]
q heat flux in a certain surface [W m^{-2}], /region/volume [W m^{-3}]
Q total heat flux [W]
s generation/consumption term [kg s^{-1}]
t time [s], thickness [m]
T temperature [°C]
u velocity [m s^{-1}]
V volume [m^3]
x value of a certain variable x
X mass fraction
y value of a certain variable y

Subscripts

b bed, backflow
c core
consum consumption
db dense bed
dev devolatilization
dry drying
e equivalent
eff effective
eq equivalent
entr entrainment
f fuel
g gas
i region, element
j thermochemical process, other surfaces
k phase component, other cells
lat lateral
m calculated in the model
p particle, measured in the plant
rad radiation
ref reference
rel relative
s bulk solids, slip
surf surface
susp suspension
t terminal
top top of the riser
vol volume
w wall layer, wall
x x-axis direction
y y-axis direction
z z-axis direction
0 at the dense bed
∞ after new steady-state is reached

Abbreviations

AP absolute percentage error
CV controlled variable
BBM black-box model
BFB bubbling fluidized bed
CFB circulating fluidized bed
CFD computational fluid dynamics
EB energy balance
FB fluidized bed
FBC fluidized bed combustion/combustor
FM fluidization model
HHV high heating value
MIMO multiple-input-multiple-output
MV manipulated variable
P&ID piping and instrumentation diagram
RC relative change
St Stokes number

■ REFERENCES

(1) Koornneef, J.; Junginger, M.; Faaij, A. Development of fluidized bed combustion — An overview of trends , performance and cost. *Prog. Energy Combust. Sci.* **2007**, *33*, 19−55.
(2) Basu, P. *Circulating fluidized bed boilers*; Elsevier, 2015.
(3) European Commission. Roadmap 2050. *Policy* 1−9 (**2012**).
(4) IEA. *Harnessing variable renewables: a guide to the balancing challenge*. (2011).
(5) Genrup, M.; Thern, M. Gas turbine developments. *Ny gasturbinteknik* **2012-2014**, 2012.
(6) Alobaid, F.; et al. Progress in dynamic simulation of thermal power plants. *Prog. Energy Combust. Sci.* **2017**, *59*, 79−162.
(7) Gómez-Barea, A.; Leckner, B. Modeling of biomass gasification in fluidized bed. *Prog. Energy Combust. Sci.* **2010**, *36*, 444−509.
(8) Gungor, A. One dimensional numerical simulation of small scale CFB combustors. *Energy Convers. Manage.* **2009**, *50*, 711−722.
(9) Yang, H.; Yue, G.; Xiao, X.; Lu, J.; Liu, Q. 1D modeling on the material balance in CFB boiler. *Chem. Eng. Sci.* **2005**, *60*, 5603−5611.
(10) Trendewicz, A.; Braun, R.; Dutta, A.; Ziegler, J. One dimensional steady-state circulating fluidized-bed reactor model for biomass fast pyrolysis. *Fuel* **2014**, *133*, 253−262.
(11) Pallarès, D.; Johnsson, F. Macroscopic modelling of fluid dynamics in large-scale circulating fluidized beds. *Prog. Energy Combust. Sci.* **2006**, *32*, 539−569.
(12) Kaikko, J.; Mankonen, A.; Vakkilainen, E.; Sergeev, V. Core-annulus model development and simulation of a CFB boiler furnace. *Energy Procedia* **2017**, *120*, 572−579.
(13) Pallarès, D.; Johnsson, F. Modeling of fluidized bed combustion processes. *Fluidized Bed Technol. Near-Zero Emiss. Combust. Gas.* **2013**, DOI: 10.1533/9780857098801.2.524.

https://dx.doi.org/10.1021/acs.iecr.0c06278
Ind. Eng. Chem. Res. 2021, 60, 3936−3956

(14) Park, C. K.; Basu, P. A model for prediction of transient response to the change of fuel feed rate to a circulating fluidized bed boiler furnace. *Chem. Eng. Sci.* **1997**, *52*, 3499−3509.
(15) Majanne, Y.; Köykkä, P. Dynamic model of a circulating fluidized bed boiler. *IFAC Proc. Vol.* **2009**, *42*, 255−260.
(16) Chen, Y.; Xiaolong, G. Dynamic modeling and simulation of a 410 t/h Pyroflow CFB boiler. *Comput. Chem. Eng.* **2006**, *31*, 21−31.
(17) Kim, S.; Choi, S.; Lappalainen, J.; Song, T.-H. Dynamic simulation of the circulating fluidized bed loop performance under the various operating conditions. *Proc. Inst. Mech. Eng., Part A* **2019**, *233*, 901−913.
(18) Arjunwadkar, A.; Basu, P.; Acharya, B. A review of some operation and maintenance issues of CFBC boilers. *Appl. Therm. Eng.* **2016**, *102*, 672−694.
(19) Peters, J.; Alobaid, F.; Epple, B. Operational flexibility of a CFB furnace during fast load change-experimental measurements and dynamic model. *Appl. Sci.* **2020**, *10*, 5972.
(20) Findejs, J.; Havlena, V.; Jech, J.; Pachner, D. Model based control of the circulating fluidized bed boiler. *IFAC Proc. Vol.* **2009**, *42*, 44−49.
(21) Zimmerman, N.; Kyprianidis, K.; Lindberg, C.-F. Waste Fuel Combustion: Dynamic Modeling and Control. *Processes* **2018**, *6*, 222.
(22) Kataja, T.; Mojanne, Y. Dynamic Model of a Bubbling Fluidized Bed Boiler. 2007, 140−148.
(23) Selçuk, N.; Degirmenci, E. Dynamic Simulation of Fluidized Bed Combustors and its Validation Against Measurements. *Combust. Sci. Technol.* **2001**, *167*, 1−27.
(24) Surasani, V. K.; Kretschmer, F.; Heidecke, P.; Peglow, M.; Tsotsas, E. Biomass combustion in a fluidized-bed system: An integrated model for dynamic plant simulations. *Ind. Eng. Chem. Res.* **2011**, *50*, 9936−9943.
(25) Suárez-Almeida, M.; Gómez-Barea, A.; Ghoniem, A. F.; Nilsson, S.; Leckner, B. Modeling the transient response of a fluidized-bed biomass gasifier. *Fuel* **2020**, *274*, 117226.
(26) Montañés, R. M.; Flø, N. E.; Nord, L. O. Dynamic Process Model Validation and Control of the Amine Plant at CO_2 Technology Centre Mongstad. *Energies* **2017**, *10*, 1527.
(27) Modelica Association. Modelica and the Modelica Association — Modelica Association. https://www.modelica.org/ (1996).
(28) Lackermeier, U.; Werther, J. Flow phenomena in the exit zone of a circulating fluidized bed. *Chem. Eng. Process.* **2002**, *41*, 771−783.
(29) Johnsson, F.; Vrager, A.; Tiikma, T.; Leckner, B. Solids flow pattern in the exit region of a CFB-furnace. Influence of geometry. in *Proceedings of the 15th international con- ference on fluidized bed combustion*, (1999).
(30) Johnsson, F.; Leckner, B. Vertical distribution of solids in a CFB-furnace. in *13th International conference on fluidized-bed combustion 719*, (1995).
(31) Stultz, S.; Kitto, J. Controls for Fossil Fuel-Fired Steam Generating Plants. in *Steam: its generation and use* 41−1, 41−21 (The Babcok and Wilcox Company, 2005).
(32) Mcbride, B. J.; Gordon, S.; Reno, M. Coefficients for Calculating Thermodynamic and Transport Properties of Individual Species. *Nasa Tech. Memo.* **1993**, *4513*, 98.
(33) Thunman, H.; Davidsson, K.; Leckner, B. Separation of drying and devolatilization during conversion of solid fuels. *Combust. Flame* **2004**, *137*, 242−250.
(34) Thunman, H.; Niklasson, F.; Johnsson, F.; Leckner, B. Composition of volatile gases and thermochemical properties of wood for modeling of fixed or fluidized beds. *Energy Fuels* **2001**, *15*, 1488−1497.
(35) Lundberg, L.; Johansson, R.; Pallarès, D.; Thunman, H. A conversion-class model for describing fuel conversion in large-scale fluidized bed units. *Fuel* **2017**, *197*, 42−50.
(36) Verheijen, F. G. A.; Zhuravel, A.; Silva, F. C.; Amaro, A.; Ben-Hur, M.; Keizer, J. J. The influence of biochar particle size and concentration on bulk density and maximum water holding capacity of sandy vs sandy loam soil in a column experiment. *Geoderma* **2019**, *347*, 194−202.
(37) Sterneus, J.; Johnsson, F. Gas mixing in the wall layer of a CFB boiler. in *Proceedings of the 14th International conference on fluidized bed combustion*, 1997.
(38) Vermeer, D. J.; Krishna, R. Hydrodynamics and Mass Transfer in Bubble Columns in Operating in the Churn-Turbulent Regime. *Ind. Eng. Chem. Process Des. Dev.* **1981**, *20*, 475−482.
(39) Lundberg, L.; Soria-Verdugo, A.; Pallarès, D.; Johansson, R.; Thunman, H. The role of fuel mixing on char conversion in a fluidized bed. *Powder Technol.* **2017**, *316*, 677−686.
(40) Johnsson, F.; Zhang, W.; Leckner, B. Characteristics of the formation of particle wall layers in CFB boilers. in *2nd Int. Conf. on Multiphase Flow, Vol 3* (1995).
(41) Djerf, T.; Pallarès, D.; Johnsson, F. Solids flow patterns in large-scale Circulating Fluidised Bed boilers: Experimental evaluation under fluid-dynamically down-scaled conditions. *Chem. Eng. Sci.* **2021**, *231*, 116309.
(42) Haider, A.; Levenspiel, O. Drag Coefficient and Terminal Velocity of Spherical and Nonspherical Particles. *Powder Technol.* **1989**, *58*, 63−70.
(43) Djerf, T. Solids flows in circulating fluidized beds: explorations of phenomena with applications to boilers. (Chalmers University of Technology, 2020).
(44) Mathekga, H. I.; Oboirien, B. O.; North, B. C. A review of oxy-fuel combustion in fluidized bed reactors. *Int. J. Energy Res.* **2016**, *40*, 878−902.
(45) Lafanechere, L.; Jestin, L. Study of a circulating fluidized bed furnace behavior in order to scale it up to 600 MWe. in *13 International conference on fluidized-bed combustion* (1995).
(46) Mirek, P. Influence of the model scale on hydrodynamic scaling in CFB boilers. *Braz. J. Chem. Eng.* **2016**, *33*, 885−896.
(47) Zhang, W.; Johnsson, F.; Leckner, B. Fluid-dynamic boundary layers in CFB boilers. *Chem. Eng. Sci.* **1995**, *50*, 201−210.
(48) Werther, J. Fluid mechanics of large-scale CFB units. *in Circul Fluid Bed Technology* **1993**, 1−14.
(49) Kang, S. K.; Kwon, T. W.; Kim, S. D. Hydrodynamic Characteristics of Cyclone Reactors. *Powder Technol.* **1989**, *58*, 211−220.
(50) Oka, S. *Fluidized bed combustion*, Marcel Dekker, Inc.: New York; (2004).
(51) Ström, H.; Thunman, H. A computationally efficient particle submodel for CFD-simulations of fixed-bed conversion. *Appl. Energy* **2013**, *112*, 808−817.
(52) Flagan, R. C.; Seinfeld, J. H. *Fundamentals of air pollution engineering*, Dover Publication INC.: Mineola New York; 2012.
(53) Westbrook, C. K.; Dryer, F. L. Simplified Reaction Mechanisms for the Oxidation of Hydrocarbon Fuels in Flames. *Combust. Sci. Technol.* **1981**, *27*, 31−43.
(54) Lide, D. R. *CRC Handbook of Chemistry and Physics*, 84th Edition, 2003-2004.
(55) Breitholtz, C.; Leckner, B.; Baskakov, A. P. Wall average heat transfer in CFB boilers. *Powder Technol.* **2001**, *120*, 41−48.
(56) Howell, J. R. *A catalog of radiation configuration factors*. (McGraw-Hill, 1982).
(57) Karlstad Energi homepage. https://www.karlstadsenergi.se/ (2020).
(58) Sandberg, J.; Fdhila, R. B.; Dahlquist, E.; Avelin, A. Dynamic simulation of fouling in a circulating fluidized biomass-fired boiler. *Appl. Energy* **2011**, *88*, 1813−1824.
(59) Leckner, B. Process aspects in combustion and gasification Waste-to-Energy (WtE) units. *Waste Manage.* **2015**, *37*, 13−25.
(60) EU. *Directive 2010/75/EU of the European Parliament and of the Council of 24 November 2010 on industrial emissions (integrated pollution prevention and control)*. vol. 25 (2010).
(61) Taler, J.; Taler, D.; Kaczmarski, K.; Dzierwa, P.; Trojan, M.; Sobota, T. Monitoring of thermal stresses in pressure components based on the wall temperature measurement. *Energy* **2018**, *160*, 500−519.

https://dx.doi.org/10.1021/acs.iecr.0c06278
Ind. Eng. Chem. Res. 2021, 60, 3936−3956